Clim. Past Discuss., 5, 1055–1107, 2009
www.clim-past-discuss.net/5/1055/2009/

Climate of the Past Discussions

Climate of the Past Discussions is the access reviewed discussion forum of *Climate of the Past*

Glacial climate sensitivity to different states of the Atlantic Meridional Overturning Circulation: results from the IPSL model

M. Kageyama[1], J. Mignot[2], D. Swingedouw[3], C. Marzin[1], R. Alkama[1,4], and O. Marti[1]

[1]LSCE/IPSL, UMR CEA-CNRS-UVSQ 1572, CE Saclay, L'Orme des Merisiers, Bât. 701, 91191 Gif-sur-Yvette Cedex, France
[2]LOCEAN, Universite Pierre et Marie Curie, Case courrier 100, 4 place Jussieu, 75252 Paris Cedex 05, France
[3]CERFACS, 42 Avenue Gaspard Coriolis 31057 Toulouse, France
[4]CNRM, 42 av Coriolis, 31057 Toulouse cedex 1, France

Received: 22 December 2008 – Accepted: 16 January 2009 – Published: 18 March 2009

Correspondence to: M. Kageyama (masa.kageyama@lsce.ipsl.fr)

Published by Copernicus Publications on behalf of the European Geosciences Union.

Abstract

Numerous records from the North Atlantic and the surrounding continents have shown rapid and large amplitude climate variability during the last glacial period. This variability has often been associated to changes in the Atlantic Meridional Overturning Circulation (AMOC). Rapid climate change on the same time scales has also been reconstructed for sites far away from the North Atlantic, such as the tropical Atlantic, the East Pacific and Asia. The mechanisms explaining these climatic responses to the state of the AMOC are far from being completely understood, especially in a glacial context. Here we study three glacial simulations characterised by different AMOC strengths: 18, 15 and 2 Sv. With these simulations, we analyse the global climate sensitivity to a weak (18 to 15 Sv) and a strong (15 to 2 Sv) decrease in the AMOC strength.

A weak decrease in the AMOC is associated, in our model simulations, to the classical North Atlantic and European cooling, but this cooling is not homogeneous over this region. We investigate the reasons for a lesser cooling (or even slight warming in some cases) over the Norwegian Sea and Northwestern Europe. It appears that the convection site in this area is active in both simulations, but that convection is unexpectedly stronger in the 15 Sv simulation. Due to the large variability of the atmosphere, it is difficult to definitely establish what is the origin of this climatic difference, but it appears that the atmospheric circulation anomaly helps sustaining the activity of this convection sites. Far from the North Atlantic, the climatic response is of small amplitude, the only significant change appearing in summer over the tropical Atlantic, where the Inter-Tropical Convergence Zone (ITCZ) shifts southward.

The climate differences between the 15 Sv and 2 Sv simulations are much larger and our analyses focus on three areas: the North Atlantic and surrounding regions, the Tropics and the Indian monsoon region. We study the timing of appearance of these responses to the AMOC shutdown, which gives some clues about the mechanisms for these teleconnections. We show that the North Atlantic cooling associated with the collapse of the AMOC induces a cyclonic atmospheric circulation anomaly centered over

CPD

5, 1055–1107, 2009

the North Atlantic, which modulates the eastward advection of the cold anomaly over the Eurasian continent. It can explain that the cooling is not as strong over Western Europe as over the North Atlantic and the rest of the Eurasian continent. Another modification in the northern extratropical stationary waves occurs over the Eastern Pacific, explaining a warming over Northwestern America. In the Tropics, the ITCZ southward shift in this simulation appears to be strongest over the Atlantic and Eastern Pacific and results from an ajustment of the atmospheric and oceanic transports. Finally, the Indian monsoon weakening also appears to be connected to the tropospheric cooling over Eurasia.

1 Introduction

Since the discovery of abrupt oceanic and climate changes in marine records from the North Atlantic (Heinrich, 1988) and glaciological records from Greenland (Dansgaard et al., 1993), numerous studies have contributed to better describe this large amplitude millenial scale variability during glacial periods. A first step, accomplished by Bond et al. (1993) was to demonstrate the simultaneity between the abrupt changes in surface ocean conditions, as characterized by changes in foraminiferal assemblages, and those in the oxygen isotopic record from Greenland. Further studies of marine proxies sensitive to the ocean ventilation (e.g. ^{13}C, Elliot et al., 2002) or circulation (e.g. paleomagnetic properties of the marine sediments, see Kissel, 2005, for a recent review) show that the North Atlantic water ventilation and circulation strongly decreased during Heinrich events, but not so much during stadials. The Atlantic Meridional Overturning Circulation (AMOC) has then logically been proposed to play a key role in causing climatic changes both around and far from the North Atlantic, and in particular in the Southern Hemisphere and Antarctica (e.g. Blunier et al., 1998; EPICA community members, 2006). Characterising the climatic changes for different states of the AMOC under glacial conditions can therefore help interpreting the numerous records of glacial millenial scale variability available for regions close or far away from the North Atlantic.

In the present study, we use a global coupled ocean-atmosphere general circulation model to study the surface climate differences related to three different states of the AMOC under glacial boundary conditions. We focus our analysis on three regions: the northern extratropics, the tropical Atlantic, and the Indian monsoon region.

1.1 Palaeorecords of the climate sensitivity to the AMOC state

Pollen records retrieved in marine sediment cores off the European coast, and in particular around the Iberian Peninsula margin, show that simultaneously to abrupt changes in sea surface conditions, the composition of the vegetation on the nearby land changed significantly (Combourieu Nebout et al., 2002; Sánchez-Goñi et al., 2002, 2008), with more forests during interstadials, characterized by relatively warm sea surface temperatures and more semi-desert or steppic vegetation during stadials, characterized by relatively cold ocean surface conditions. These vegetation changes have been interpreted in terms of climate, in particular in terms of temperatures of the coldest month and annual precipitation (Sánchez-Goñi et al., 2002) which vary synchronously with the variations in surface ocean characteristics recorded in the same cores. Other types of continental records, such as the speleothem record from Villars Cave in Southwestern France (Genty et al., 2003), confirm the abrupt and large amplitude climatic and vegetation changes during the last glacial period. Schematically, these records suggest cold and dry stadials, and warmer and wetter interstadials over Southwest Europe. Additional information on the atmospheric circulation of this region has been obtained from a clay mineral record from the Alboran Sea (Bout-Roumazeilles et al., 2007) which shows more export of dust from Morocco to the Mediterranean Sea during stadials and even more prominently during Heinrich events, which can be related to a more southerly circulation during these periods in this region. This signature associated with cold conditions over the North Atlantic constrasts with the warm, wet conditions found during Heinrich events on the other side of the Atlantic, in Florida (Grimm et al., 2006). This shows that even around the North Atlantic, the continental climate response to cold oceanic conditions and/or to a weakening of the AMOC is far from

CPD
5, 1055–1107, 2009

being spatially homogeneous. Furthermore, studying an apparent mismatch between reconstructions of the Greenland temperatures based on ice core and on snowline changes, Denton et al. (2005) show that the climatic response to a weakening of the AMOC is likely to be dependent on the season, with the strongest cooling occuring in winter.

Abrupt climatic variations have also been recorded, on the same type of time-scales as for the events occuring around the North Atlantic, away from from this region. Records from the tropical Atlantic (e.g. Cariaco Basin, Peterson et al., 2000; González et al., 2008) show dry events during Greenland stadials, while to the South of these sites, in North East Brazil, wet events are recorded (Wang et al., 2004). Taken together, these records can be interpreted as showing a southward migration of the Intertropical convergence zone (ITCZ) during stadials over the Atlantic Basin. This is confirmed for the other side of the tropical Atlantic by dusty events recorded off the northwestern African margin during Heinrich events (Jullien et al., 2007), which suggest southward shifts of the ITCZ during those events. Leduc et al. (2007) further suggest this southward migration to be associated with a decrease in moisture transport from the Atlantic to the Pacific, due to the topographic barrier of the Andes. They hypothesize that a decreased moisture transport from the Atlantic to the Pacific causes a salinity decrease in the tropical Western Atlantic, which, once advected to the North Atlantic convection sites, acts to further weaken the AMOC. The southward migration of the ITCZ during stadials is therefore supported by many records. Such a migration is also suggested for the Western Pacific during Heinrich events from records from North East Australia (Turney et al., 2004; Muller et al., 2008).

Speleothem and loess records from China show that the East Asian monsoon also shows strong millenial scale variations, with decreases in the summer monsoons during Heinrich events and stadials (Porter and An, 1995; Wang et al., 2001). Ruth et al. (2007), analysing the dust content from the ice cores retrieved by the North Greenland Ice Core Project, suggest a very tight temporal correspondance between the climatic changes recorded in Greenland and the East Asian monsoon activity, which modu-

lates the dust archived in Greenland. Several records show that the Indian monsoon intensity also changes in glacial times, simultaneous with Greenland stadials and interstadials (Schulz et al., 1998; Leuschner and Sirocko, 2000; Altabet et al., 2002; Rashid et al., 2007). In addition, Sánchez-Goñi et al. (2008) show a correspondance between the impacts of Dansgaard-Oeschger events in western Europe and in Asia. Variations in Asian monsoon strength could be responsible for the abrupt changes in atmospheric methane concentration recorded in ice cores both from Greenland and Antarctica (Blunier et al., 1998; EPICA community members, 2006).

In summary, millenial-scale variability, first revealed in records of North Atlantic surface conditions and in Greenland ice core records, is traced in many paleo-records around the world. Changes in the global ocean circulation, and in particular in the AMOC, are often invoked as the main mechanism responsible for these teleconnections.

1.2 Insights from numerical models

This idea is supported by models which have shown that the thermohaline circulation (here assimilated to the AMOC) is characterised by several equilibria (Stommel, 1961) and that transitions between these equilibria, i.e. between situations in which the AMOC is slow or shut-down and situations with strong AMOC, can be rapid (Rahmstorf, 1994). Using an atmospheric-ocean coupled General Circulation Model (AOGCM) and forcing its AMOC from an "on" state, similar to the present one, to on "off" state, and back to an "on" state, Manabe and Stouffer (1995) showed that it was possible to simulate an abrupt climate change in the North Atlantic, which they related to be similar to the Younger Dryas. They showed that a strong temperature anomaly develops over and around the North Atlantic in response to a weakening of the thermohaline circulation but that no strong temperature anomaly develops elsewhere. This type of experiments, termed "water-hosing experiments", have been run by many groups since then, with models of different complexities. Stouffer et al. (2006) compile the results from 14 models in which a fresh water flux of 0.1 and 1 Sv is applied in the North At-

lantic between 50 and 70° N. All models simulate, to various degrees, a weakening of the AMOC and a cooling of the North Atlantic in response to the 0.1 Sv fresh water flux, but some models also simulate a warming in the Nordic and/or Barents Sea. The response to the 1.0 Sv fresh water flux in the North Atlantic, Nordic Seas and Arctic Ocean is a general cooling, which is maximum over the North Atlantic and Nordic Seas between 50 and 80° N. This shows the sensitivity of the climate response to different fresh water forcings and different states of the thermohaline circulation. In addition, a recent study by Saenko et al. (2007) shows that if the fresh water flux is introduced along the northeastern coasts of the North Atlantic, and not uniformely over the 50–70° N band, the response to this freshwater flux is much more complex. It involves a warming over some areas of the North Atlantic, due to changes in ocean currents caused by the density anomalies due to the fresh water input, even if at the same time the AMOC itself weakens.

The climatic sensitivity to a collapsed AMOC (1 Sv fresh water experiment), as depicted by the results compiled by Stouffer et al. (2006), include a cooling over the extratropical North Atlantic ocean (the amplitude and extent of this cooling is model-dependent) which propagates over Eurasia. The cooling is not as strong over North America. The response to a 0.1 Sv fresh water flux to the North Atlantic is of smaller amplitude but studied more comprehensively. In terms of atmospheric circulation, the North Atlantic sea surface temperature (SST) anomaly is associated with a cyclonic sea-level pressure anomaly, which constitutes a modulation of the mid-latitude westerlies. A collapse in the AMOC therefore has an impact on the Northern Hemisphere stationary wave pattern. Vellinga and Wood (2002) show that this response appears within decades of their initial (very strong) perturbation. They also obtain a cyclonic anomaly over the northern North Atlantic, with southwesterly surface wind anomalies over western Europe. This could explain why the temperature anomalies over this region are not as strong as over the North Atlantic. Relatively warmer air is advected by the anomalous circulation forced by the North Atlantic cooling.

The SST response in areas remote from the North Atlantic is dominated by a warm-

ing of the South Atlantic and of the Southern Ocean. This follows the classical interhemispheric (bipolar) see-saw effect (Stocker, 1998), which appears more prominently in the Atlantic. This creates, around the Equator, a temperature anomaly dipole, with colder waters to the North and warmer waters to the South when the AMOC is weaker. This dipole is associated with a southward shift of the ITCZ (Chiang et al., 2008). The development of such a dipole is due to a decrease in interhemispheric transport of heat by the Atlantic ocean. The atmosphere also plays a role. Chiang and Bitz (2005) and Yang and Liu (2005) show that an imposed cooling in the North Atlantic propogates towards the Equator and cools the SST to the South through a Wind-Evaporation-SST feedback (Chiang et al., 2008). When the anomalous winds pass the Equator, they change their direction and tends to warm the SSTs, amplifying the dipolar SST anomalies and the ITCZ shift.

The monsoon response to an AMOC weakening is consistent with a southward shift of the ITCZ. However, specific mechanisms have been suggested which could play a role in the monsoon variations concommittant with the millenial scale events occuring in the North Atlantic. On the basis of observational data from 1871 to 2003, Goswami et al. (2006) propose that the Indian summer monsoon and Atlantic Multidecadal Oscillation (AMO) could be linked via a modification of the meridional gradient of the temperature of the upper half of the troposhere (which they term "TT"). They show that for a warm North Atlantic, there is an increase in the meridional gradient of TT, which, in turn, favours a stronger monsoon. Using a coupled ocean-atmosphere model on which they impose a positive sea surface temperature anomaly in the North Atlantic, Lu et al. (2006) show that in addition to the atmospheric connection via the TT meridonal gradient, coupled ocean-atmosphere feedbacks in the Indian and Western Pacific Ocean help instensifying the monsoon. Indeed, the warm anomaly in the North Atlantic is associated with warm anomalies in the Indian and western Pacific oceans, which help producing more precipitation and induce an enhanced monsoon circulation. Zhang and Delworth (2005) show that the weakening of the East Asian monsoon in their coupled GCM with a weaker AMOC is related to a change of the Pacific Walker circulation and

the Rossby wave response to the resulting dampened convection over Indonesia acts to weaken the Indian monsoon.

All the experiments cited above were run in the present-day or pre-industrial contexts, i.e. for present or pre-industrial greenhouse gas concentrations and ice-sheet extent and topography. On the other hand, millenial scale variability is largest during glacial times. Using a climate model of intermediate complexity, Ganopolski and Rahmstorf (2001) show that a glacial climate is much more sensitive to fresh water fluxes in the North Atlantic than an interglacial climate. Hu et al. (2008), using a fully coupled ocean-atmosphere general circulation model, show that when the Bering Strait is closed, the recovery of the AMOC from an "off" to an "on" state is slower, due to the fact that the fresh water introduced in the North Atlantic takes a longer time to be removed from this region when the Arctic and Pacific oceans are not connected.

In terms of glacial surface climate response to a collapse in the AMOC, Ganopolski and Rahmstorf (2001), along with the follow-up studies of Claussen et al. (2003) and Jin et al. (2007), show a cooling of the North Atlantic, extending over Eurasia, and a smaller cooling over the Pacific and North America. The response in the Southern Hemisphere is an overall warming, consistent with the bipolar see-saw mechanism. In addition, using the same model, Jin et al. (2007) show that the decrease in Eurasian temperatures associated with a weakening of the AMOC can be responsible for a weakening of the Asian monsoon. The thermal response to a collapse of the AMOC simulated by the HadCM3 fully coupled atmosphere-ocean general circulation model (Hewitt et al., 2006) is broadly consistent with the results of the CLIMBER climate model of intermediate complexity.

Using the coupled ocean-atmosphere model ECBILT-CLIO forced with full glacial boundary conditions, Timmermann et al. (2005) and Krebs and Timmermann (2007) investigate the mechanisms for the teleconnections between the North Atlantic oceanic state and equatorial Pacific temperatures and salinities, during a transient meltwater pulse experiment in which the AMOC shuts down and recovers. Analysing fully coupled as well as partially coupled atmosphere-ocean simulations, they examine the respec-

tive roles of the atmosphere and the ocean in the response to the AMOC collapse. They find that the North Atlantic cooling associated with the AMOC collapse is advected downstream over the Eurasian continent and is largely responsible, on its own, for the atmospheric circulation changes simulated in their coupled experiments. This includes a weakening of the Asian monsoon and an intensification of the trade winds over the northern tropical Pacific, both related to changes in the meridional temperature gradient. In addition, the ocean responds to the fresh water flux imposed in the Atlantic and the associated sea-level increase via a standing wave pattern which has a global impact on the thermocline structure. In the Western Pacific, this adjustment involves the transport of cold and salty waters in the Pacific warm pool, a response which is further amplified by the fact that trade winds intensify and precipitation decrease in this area.

Flückiger et al. (2008) use the same model to show that the surface climate response to an increase in AMOC is not linear with respect to the AMOC strength. They also show that the surface climate response to an AMOC intensification is dependent on the season, with the high northern latitudes undergoing the maximum climate changes in winter while the differences over the mid-latitude Eurasian continent are largest in spring due to a shift of the period of snow retreat. This, in turn, is responsible for an earlier break of the Siberian high pressure and an earlier setup of the Asian monsoon. The dependence of the climate response on the season has important implications for the interpretation of proxy data, as they are often more sensitive to the climate of one particular period of the year.

Hence, to our knowledge, there are not many more fresh water hosing experiments run in the glacial climatic context, with fully coupled ocean-atmosphere general circulation models. In this study, we report on new results obtained with the IPSL_CM4 model. We consider the surface climate sensitivity to a weak change in an active AMOC (18 vs. 15 Sv) and to a collapse of the AMOC. By comparing the climatic responses to these changes, we show that the surface climate response to an AMOC change is not linear. We also examine the seasonality, timing, and mechanisms of the northern extratropical

climate responses to both these AMOC changes (Sect. 4.2). By analysing the surface climate anomaly associated with an AMOC collapse and its timing, we look for possible mechanisms of teleconnections between the North and tropical Atlantic (Sect. 5.1), as well as between the North Atlantic and the Indian monsoon (Sect. 5.2).

2 Description of the climate model simulations

In order to study the climate differences associated with different states of the AMOC in a glacial context, three simulations have been performed with the coupled ocean-atmosphere IPSL_CM4 model (Marti et al., 2006, 2008). The atmospheric component of this coupled model is LMDZ.3.3, with resolution 96×71×19 in longitude×latitude×altitude. The horizontal grid is regular, while the vertical levels are more numerous near the surface. This atmospheric modules includes the land surface scheme ORCHIDEE, in which the river routine has been adapted for Last Glacial Maximum (LGM) conditions (Alkama et al., 2008). The ocean module is ORCA2, which uses an irregular horizontal grid of 182×149 points with a resolution of ca. 2°, refined over key regions such as the North Atlantic and near the Equator. This model has 31 depth levels. The sea-ice module is the Louvain Ice Model (LIM), developed at Louvain-La-Neuve. The coupling of these components is performed using the OASIS (version 3) coupler.

For all three simulations the boundary conditions are the same and correspond to the PMIP2 set-up for Last Glacial Maximum simulations (Braconnot et al., 2007; http://pmip2.lsce.ipsl.fr): we use the ICE-5G ice-sheet reconstruction for the ice-sheets (Peltier, 2004), CO_2, CH_4 and N_2O atmospheric concentrations of 185 ppm, 350 ppb and 200 ppb, respectively (following Monnin et al., 2001; Dallenbach et al., 2000; Flückiger et al., 1999), and orbital parameters relevant for 21 ky BP (Berger, 1978). Runs LGMa and LGMb have been initialised from a previous LGM simulation and run for 250 years. Run LGMc starts from year 150 of LGMb and has been run for 420 years, hence stopping at year 150+420=570 on the timescale of simulations LGMa and b

CPD
5, 1055–1107, 2009

(Fig. 1). In all simulations, snow accumulates on the ice-sheets and this fresh water sink has to be compensated in order to obtain stable simulations. In order to do so, three latitude bands are defined, with limits at 90° S/50° S/40° N/90° N. The 40° N limit roughly corresponds to the southernmost latitudes reached by icebergs during ice ages. In each latitude band, the excess freshwater accumulating as snow on the ice sheets, which we define as "calving", is integrated and supplied to the ocean in the same latitude band. For the northern band, freshwater fluxes due to calving are delivered to the Atlantic and Arctic Oceans, but not to the Pacific. In all three simulations, there is a remaining imbalance in the fresh water budget due to a slightly non conservative atmospheric convection scheme. In simulations LGMa and LGMb, the fresh water budget is closed using different methods. For LGMa, this bias is compensated for by multiplying global precipitation by 2.1%. In LGMb, the calving flux is multiplied by 44%. As a result, both LGMa and LGMb have a closed fresh water balance. In LGMc, the calving flux has been multiplied by 100%, the fresh water balance is not closed.

3 Response of the Atlantic Meridional Overturning Circulation and global climatic consequences

3.1 Evolution of the Atlantic Meridional Overturning Circulation and global heat transport adjustments

The perturbation in fresh water flux into the northern North Atlantic and Arctic are of 0.08 Sv between LGMa and LMGb and of 0.1 Sv between LGMb and LGMc. They are therefore of similar magnitude and are stable during all the simulations (not shown). Yet, while LGMa and LGMb present strong and stable AMOCs, with strengths 18 and 15 Sv respectively, the AMOC collapses to 2 Sv by the end of simulation LGMc (Fig. 1). The analyses presented in this work are primarily based on the statistics for years 201 to 250 of runs LGMa and b, and for years 371 and 420 of LGMc, i.e. when its AMOC has collapsed. For these periods, the AMOC for the three simulations is represented

on Fig. 2. In LGMa and b, the North Atlantic Deep Water (NADW) formation is strong and the NADW cell reaches the bottom of the North Atlantic Ocean in the northern mid-latitudes. This contrasts with the AMOC in run LGMc, which has completely collapsed. Hence the ocean circulation reached in our equilibrium runs LGMa and LGMb is extremely sensitive to an increase of fresh water flux in the Northern North Atlantic, even if this additional flux is on the low side of the usual fresh water hosing experiments, which traditionally use a 1 Sv and/or a 0.1 Sv additional flux between 50 and 70° N in the North Atlantic (e.g. Stouffer et al., 2006). We can therefore conclude that the atmosphere-ocean state in LGMb is close to a North Atlantic fresh water threshold for which the AMOC collapses rapidly: although the additional fresh water in the North Atlantic is rather small, the AMOC collapses in 300 years. We therefore obtain two simulations with extreme AMOCs, one in the "on" state (LGMa) and one in the "off" state (LGMc) and a simulation (LGMb) with an active AMOC slightly smaller than the LGMa maximum. In Sect. 4.1, we take a further step in understanding these AMOC differences. We now briefly describe the global heat transport adjustments when the AMOC weakens in LGMc and the sensitivity of the mean annual climate to changes in the AMOC.

The shutdown of the AMOC in LGMc as compared to LGMb induces an important weakening in oceanic heat transport. On Fig. 3, we see that the global meridional oceanic heat transport is reduced by more than 0.32 PW when averaged between 10° S to 60° N. This decrease is lower than the 0.45 PW reduction in the Atlantic meridional heat transport, related to the shutdown of the AMOC. The other basins therefore compensate part of the reduction in the Atlantic heat transport. This reduction reaches more than 0.68 PW at 17° N or a 70% decrease in the Atlantic meridional heat transport in LGMc compared to LGMb. Figure 3 shows that the atmospheric meridional heat transport increases in response to the decrease in oceanic meridional heat transport. This type of effect has been firstly depicted by Bjerknes (1964) and is therefore usually called the "Bjerknes compensation" effect (Shaffrey and Sutton, 2006). In order to have a perfect compensation, a constant radiative budget and no storage in any heat reser-

CPD
5, 1055–1107, 2009

voirs are required. These hypotheses are scarcely verified, and here we see that the atmospheric heat transport compensation is not total, showing that the climate system has modified its radiative budget and heat storage in response to the changes in the AMOC. These modifications in radiative budget are notably due to changes in sea ice cover that modifies the albedo and therefore the radiative budget (Winton, 2003). Here the compensation represents approximately 50% in terms of meridional heat transport averaged between 10° S and 60° N. Changes in ocean and atmosphere heat transports between LGMa and LGMb are small compared to those associated to a collapse of the AMOC. At this scale, there is no compensation between the anomalies in oceanic and atmospheric heat transports.

3.2 Global features of the mean annual surface climate response

As expected from previous model results and from the heat transport changes discussed in the previous section, the North Atlantic Ocean is cooler when the AMOC is weaker. In LGMb, compared to LGMa (Fig. 4, middle), this cooling is only significant at mid-latitudes and does not exceed 2°C. In LGMc, nearly the whole North Atlantic, from 10° N northward, together with the Arctic Ocean, are much colder than in LGMb (Fig. 4, bottom). The surface air temperature cools by more than 5°C over regions in which sea ice appears in LGMc, i.e. just south of Iceland, and up to 4°C in the mid-latitude North Atlantic. Still in the northern hemisphere, Eurasia is slightly cooler in LGMb compared to LGMa, with a maximum difference of 1°C centered over Eastern Europe. The LGMc–LGMb cold anomaly is twice as strong in amplitude but nearly covers the whole Eurasian continent.

There are also regions which, in our simulations, experience a warming for a weaker AMOC. In LGMb compared to LGMa, the surface air temperature over the Norwegian Sea warms up by around 1°C. In LGMc, compared to LGMb, the region south of the Norwegian Sea, between present-day England and Norway, does not cool as much as the surrounding regions, to the West or to the East. In fact, the changes in temperature between LGMb and LGMc are not significant over this region. The western Pacific and

northeastern North America experience a warming of 1°C in LGMc compared to LGMb. In addition, the South Atlantic Ocean warms up by as much as 2°C, which, together with the North Atlantic cooling, constitutes a classical bipolar see-saw response. The Indian and Western Pacific sections of the Southern Ocean also warm up in LGMc compared to LGMb, while the eastern Pacific section of the Southern Ocean cools by as much as 2°C. A cooling of around 1°C is also found in LGMb compared to LGMa over the Southeastern Pacific and East of the Antarctic peninsula.

Hence a weak reduction of the AMOC from 18 Sv (LGMa) to 15 Sv (LGMb) is associated with significant temperature anomalies of regional extent, while a strong reduction of the AMOC, from 15 Sv (LGMb) to 2 Sv (LGMc), has a global imprint on the mean annual temperatures. The temperature response is clearly not linear w.r.t the AMOC strength in agreement with Swingedouw et al. (2008). One particular feature which we discuss further in Sect. 4.1 and 4.2 is the surprising warming over the Norwegian Sea in LGMb compared to LGMa, and the absence of strong cooling over northeastern Europe in LGMc compared to LGMb.

In terms of mean annual precipitation (Fig. 5), the LGMb–LGMa anomalies are not statistically significant. However, in LGMc compared to LGMb, there is a significant drying of the North Atlantic mid-latitudes, Western Europe and the northern Mediterranean coast, by up to 0.6 mm/day, which represents a 20% reduction in annual rainfall over these regions. The Gulf of Mexico and surrounding regions, as well as the Atlantic Ocean off Florida also experience a major decrease in precipitation. The pattern of this anomaly, which straddles Central America over the adjacent Pacific and Atlantic oceans (Fig. 5), is not associated with an underlying temperature anomaly (Fig. 4), especially over the tropical Northeastern Pacific. This suggests a change in atmospheric dynamics to be responsible for the large precipitation reduction. On the other hand, over the Northeastern Pacific and the northwestern North American coast, the precipitation increases by up to 0.8 mm/day. Over the Indian sub-continent and surrounding ocean, the rainfall also decreases, indicating a weakened Indian monsoon. Finally, the largest change in the hydrological cycle is found in the tropical Atlantic where the

CPD
5, 1055–1107, 2009

ITCZ clearly shifts southward. Indeed, a drying centered at around 10° N, the mean ITCZ location in LGMb, is accompanied by a wettening centered at around 10° S and extending over eastern Brazil. All in all, the climate differences between LGMb and c, i.e. between glacial climates with an "on" and an "off" AMOCs, are reminiscent of the climate variations during the abrupt events recorded for the last glacial period and presented in Sect. 1.

3.3 Timing of the response in the AMOC "off" state simulation

The timing of the heat transport change while the AMOC weakens in LGMc is fast both for the ocean and for the atmosphere. Figure 6 shows that within a few decades, changes appear in the Atlantic heat transport that begin to be (partly) compensated by the atmosphere after a few years. In about 70 years, the Atlantic heat transport at 17° N has decreased by more than 0.34 PW, i.e. a half of its final decrease. This timing pleads for a very rapid atmospheric adjustment to the North Atlantic cooling as observed by Yang and Liu (2005). Shaffrey and Sutton (2006) also show that the Bjerknes compensation is very fast and can be observed for inter-annual variations of the heat transport. Moreover, Fig. 6b shows that the compensation by the atmospheric heat transport vanishes North of 40° N. This is related to a change in the radiative forcing at these high latitudes associated with an increased sea-ice cover.

We can compare this timing of atmospheric and oceanic transport changes to the timing of the appearance of surface climate anomalies. Indeed, the difference in mean annual surface temperature associated with a collapse of the AMOC depicted on Fig. 4 does not appear at the same rate in every region of the globe. Figure 7 (top) shows, for each point, the year after which half of the final anomaly represented on Fig. 4 is reached, and for which the anomaly remains larger than this threshold for at least 50 years. This map is restricted to the regions north of 20° S since all regions on which our work focuses are contained in this area. The first regions which experience climate changes in LGMc compared to LGMb are the mid-latitude western and central North Atlantic and the coastal areas of the Arctic Ocean. In these regions, the threshold of

50% of the final response is reached in less than 60 years after the beginning of the run (regions in blue). By this time, the AMOC is reduced by about 5 Sv (from 15 to 10 Sv at year 210 on Fig. 1's common timescale). Before 120 years (regions in green), Greenland, the Arctic Ocean, the mid-latitude North Atlantic from 30° N northward, the African coast of the tropical Atlantic pass the threshold, as well as the whole Eurasian continent and North Africa North of 10° N. The mean annual temperature response over the tropical South Atlantic also starts to appear. The next regions for which climate anomalies pass over the 50% threshold are the tropical North Atlantic and the South Atlantic between 10 and 20° S (by year 200). By that time, the AMOC is already less than 5 Sv. The anomalies over the small region of the North Atlantic south of Greenland and Iceland, i.e. near the main convection sites (Irminger and Labrador) in LGMb, only pass the 50% threshold at around year 240. This corresponds to the shut down of these sites (cf. Fig. 10 and Sect. 4.1). Finally Northeastern Pacific and Northwestern America undergo the warming shown on Fig. 4.

This pattern suggests (1) a propagation of the temperature anomalies from the central North Atlantic around the subtropical gyre along the coasts of Africa, before the temperature cools down in the North Atlantic low latitudes; (2) a very fast climatic response over the Arctic and Northern Eurasia, which is probably related to an atmospheric stationary wave change amplified by the sea-ice and snow-albedo feedbacks; (3) an extension of this cooling over most of Eurasia and North Africa; (4) relatively slower ocean responses for the largest convection site of the Nortwestern North Atlantic, for the South Atlantic and, finally, for the Northwestern Pacific. For each step in the temperature response depicted above, we have given the corresponding AMOC value. However, this does not mean that the AMOC has to pass below this value to obtain the described response. Indeed, the climatic response over some regions such as the North Atlantic sub-tropical gyre are indirectly related to the slow down of the AMOC, via a propagation of the first cooling of the mid-latitude Western and Central Atlantic around the gyre. It is however not possible, from our experiments, to strictly disentangle the direct and immediate response to an AMOC decrease from the propagation of

CPD
5, 1055–1107, 2009

a signal advected from another region.

Over the North Atlantic and Western Europe, the timing of the precipitation response (Fig. 7, bottom) is generally very much in phase with the temperature one (Fig. 7, top). The precipitation anomaly passes over the 50% threshold before year 60 for the western and central North Atlantic, before year 120 for the rest of the mid-latitude North Atlantic and the latest response occurs over the Greenland-Iceland convection site by year 240. This suggests a direct role of temperature anomalies on precipitation, the most simple mechanism for this link being via a reduction in evaporation. This type of response also occurs in our glacial ocean-atmosphere simulation in response to changes in river run-off (Alkama et al., 2008). The response over Central America, the Gulf of Mexico and the eastern equatorial Pacific appears by year 120–180 of LGMc, i.e. before the temperature anomaly passes the 50% threshold. Over the northeastern Pacific and northwestern America, the precipitation anomaly appears in two stages. The southern part of the anomaly appears by year 120, while its northern part appears quite late, by year 240, similar to the temperature anomalies. This suggests a first response related to atmospheric circulation changes, before a response to the later temperature anomalies sets in. Over the Arabian Sea and Indian sub-continent, which are the Indian monsoon regions in our simulation (cf. Fig. 5a), the main drying appears by year 120, but a secondary decrease occurs around the Bay of Bengal by year 240. Again, this suggests a first response related to changes in atmospheric circulation (cf. Sect. 5.2) before a second, more local mechanism, adds on to this first anomaly. Changes in precipitation in the tropical Atlantic also appear gradually, with the dipole associated with the shift of the ITCZ finally setting in at around year 200 (red colour bands across Northern South America and red zone over Eastern Brazil). The mechanisms and timing of the ITCZ shift are detailed further in Sect. 5.1.

In the following sections, we first investigate the reasons for the AMOC differences between the three simulations (Sect. 4.1). We then study the mechanisms underlying the climate response over three areas: (1) the northern extra-tropics, with the contrasted response over the North Atlantic and Eurasia on the one hand and over the

Western Pacific on the other (Sect. 4.2), (2) the tropical Atlantic, over which the ITCZ shifts southward (Sect. 5.1) and (3) the Indian monsoon weakening (Sect. 5.2).

4 The northern extratropical responses

4.1 Response of oceanic deep convection in the Northern North Atlantic

Figure 8 shows the maximum mixed layer depth reached during winter in each simulation. In LGMa, North Atlantic Deep Water (NADW) formation essentially takes place North of Newfoundland and south of Iceland, immediately southward of the winter ice edge, as well as in the Arctic Ocean beneath the sea ice. Some relatively deep mixed layers are also detected along the Norwegian coast. In LGMb, deep water formation disappears from the Arctic Ocean while it tends to increase in the northern North Atlantic areas. Since this occurs simultaneously with a global reduction in AMOC strength, it suggests that deep water formed in the Arctic in the LGMa simulation actually plays an important role in this interhemispheric water transport. Figure 9 illustrates that in the Southern Labrador Sea, an anomalous mixed layer depth pattern, consisting in a southward shift of the convection site (black contours) develops in LGMb compared to LGMa. This is associated with an increase of sea ice cover in the northwestern part of the area (pink contours) that leads to a net oceanic freshwater loss downstream of this ice formation area (blue colors). This freshwater loss locally overwhelms the freshwater input due to the experimental set-up (not shown). Thus, surface water density tends to increase locally and this favours deep water formation. A similar process is at play southwest of Iceland, although the sea ice anomaly and the ice to ocean freshwater flux are much weaker. Along the Norwegian coast, deep water formation clearly decreases at around 75° N while it increases locally around 65°N. In this area, the sea ice coverage decreases, pushed by anomalous southerly winds (not shown).

Figure 10 (left hand side) illustrates the timescale on which these deep convection

changes set up in LGMb. The shallowing of the mixed layer in the Arctic area and off the Norwegian coast settles within the first years of the simulation. Changes in the subarctic areas are on the other hand delayed and settle after several decades. In these areas, the interannual variability also clearly increases. This suggests a link with a change in atmospheric variability but the coupled simulations make it difficult to isolate the exact mechanism. However, it raises the possibility for delayed climatic responses to changes in the North Atlantic freshwater budget that can have important regional consequences.

As expected from Fig. 1, NADW formation is practically shut off in LGMc, which experiences the strongest input of freshwater in the northern North Atlantic compared to LGMa and b (Fig. 8, bottom). The AMOC reduction is also associated to a southward displacement of the winter sea ice edge. This results from a direct capping of the deep water formation sites by the freshwater. As above, all convection sites do not cease their activity at the same time: while the Norwegian Sea convective activity immediately decreases after the start of the run and completely cease in less than 100 years, the Labrador Sea site remains very variable, sometimes reaching the activity levels of LGMb, over the first hundred years of LGMc, before shutting off. The slowest site to react is the one in the Irminger Sea and south of Iceland, which finally shuts off after 200 years of simulation. This could be related to the fact that for this site, the mixed layer is the deepest (ca. 1000 m), and that it is the least variables of the three sites in LGMb. Indeed the Norwegian Sea mixed layer depth sometimes reaches 1000 m but is a lot more variable.

4.2 Surface climate impacts

We have shown the mean annual surface climate response on Figs. 4 and 5 and discussed this response, along with its timing, in Sects. 3.2 and 3.3. Figures 11 and 12 show the seasonal dependence of the differences due to a weak (LGMb–LGMa) and to a strong (LGMc–LGMb) perturbation. As argued by Denton et al. (2005), it is important to study the seasonal variations of the climatic response because climate proxies are

not all sensitive to a mean annual climate parameter. It also brings elements towards the understanding of the mean annual climate differences, which can be related to a season-dependent mechanism.

The difference in temperature between LGMa and LGMb over the North Atlantic (Fig. 11, l.h.s.) is rather constant over the year. This anomaly is associated to changes in the stationary waves in these seasons, as shown by the presence of a cyclonic anomaly over the zone of cooling. This structure can be traced from the sea surface to the 200 hPa level and is shown for the 500 hPa level on Fig. 13 (middle). If we compare the location of this cyclonic anomaly to the mean flow on Fig. 13 (top), we can see that it corresponds to a southward shift of the jet-stream, which is consistent with the cooling inducing the strongest meridional temperature gradient more to the south than its position in LGMa. This anomaly can explain that the North Atlantic cooling does not expand over western Europe, which undergoes southerly wind anomalies.

Over Northern Eurasia, another cyclonic anomaly develops, bringing cold air from the North over Central and Eastern Europe. This cyclonic anomaly occurs for autumn and winter, consistent with the cooling simulated over these regions for these seasons. It is not possible, from our experiments only, to determine if the cyclonic anomaly over the North Atlantic is responsible for the Eurasian cyclonic anomaly via a disturbance of the autumn and winter stationary waves, or if the Eurasian cyclonic anomaly develops as a response to the cooling over this area. However, the surface temperature anomaly and associated atmospheric circulation anomalies seem to act as if they sustain each other. The warming over the Norwegian Sea mainly occurs in the transition seasons. It does not correspond to an anomaly in the sensible heat transport (which structure, not shown, is very similar to the 500 hPa wind), hence confirming the rather local mechanism, developed in Sect. 4.1, based on changes in sea ice cover and surface winds. Precipitation differences between LGMa and LGMb are scarcely significant and will not be discussed further.

Changes in atmospheric circulation also appear to play an active role in setting up the thermal response to a strong decrease in AMOC, from LGMb to LGMc. A cyclonic

CPD
5, 1055–1107, 2009

anomaly develops over the region of strongest cooling of the North Atlantic, i.e. over the Northeastern North Atlantic. This anomaly brings energy to Northwestern Europe, hence explaining the relatively low cooling over this region (Fig. 13, bottom). Consistent with this, an anticyclonic anomaly centered over the Central Mediterranean brings colder air to Central and Eastern Europe, explaining the local maximum cooling there. Hence the cooling of Eurasia is not only explained by advection of cold air from the North Atlantic by the westerlies. Superimposed to this response, the cyclonic circulation forced by the initial cooling over the North Atlantic ocean brings warmer air to Western Europe and limitates the cooling there, while the cooling is amplified by cold air advection further east over Central and Eastern Europe. This behaviour is more pronounced in winter and spring in the temperature response shown on Fig. 11. This is consistent with the atmospheric circulation behaviour, which is similar for winter and spring (cf. Fig. 13, bottom) but with much less pronounced stationary waves over Eurasia in summer and autumn.

The precipitation response over the North Atlantic and Europe also depends on the season, partly because the precipitation in the LGMb (Fig. 12, l.h.s.), as for the present observed situation, is highly seasonal. Over the Northern Atlantic Ocean, the decrease in precipitation is maximum, in extent and amplitude, in winter and minimum in summer. This drying is strongest over the eastern side of the basin, where the cooling is also the largest. This points to a simple relationship between North Atlantic temperature and precipitation anomalies, via a decrease in evaporation (Fig. 14). Over the northern Mediterranean area, the decrease in precipitation is strongest in winter, while in Western to Central Europe, north of the Mediterranean, the drying is strongest in autumn. For these 2 regions, the strongest response therefore occurs at the season for which the precipitation is maximum in the reference run.

The temperature response to an AMOC collapse is rather constant throughout the year over the Eastern Pacific and Northwestern America, which undergo a warming (Fig. 11). There are no temperature differences in the rest of the extratropical Pacific. This warming can be explained by a cyclonic anomaly, present at all seasons, extend-

ing from the dateline to the west American coast and from ca. 30 to 60° N. The precise position and intensity of this cyclonic anomaly slightly change from season to season but its net effect is that southwesterly winds bring warmer air to the Northeastern Pacific and Northwestern America. This warming is accompanied by an increase in precipitation, which is strongest, in amplitude and extent, in summer and autumn. This phenomenon is not only related to evaporation anomalies, as for the North Atlantic Ocean (Fig. 14), but also to the southward shift of the westerlies and storm-tracks which is prominent in summer and autumn.

5 Climate response to a reduced AMOC in the Tropics

5.1 Atlantic inter tropical convergence zone

The modifications in atmospheric heat transport described in Sect. 3.1 occur via an adjustment of the meridional cells in the atmosphere. In LGMb, the atmospheric zonally averaged meridional streamfunction (Fig. 15, contours) shows a near symmetry about the Equator, with two Hadley cells located approximately from the Equator to the 30° N or S. The limit between these cells lies at around 4° N and they are therefore not strictly symmetric about the Equator. Poleward of the Hadley cells, the Ferrel cells, between 30 and 50° N or S and finally the polar cells, mostly active in the Northern Hemisphere, are simulated. The differences between LGMc and LGMb affect every cell (Fig. 15, colour shading). The largest differences are nonetheless located near the Equator where a large positive (clockwise) anomaly implies a southward shift of the limit between the two Hadley cells. This shift amounts to around 10° of latitude. This type of adjustment in response to an imposed northern hemisphere cooling is in agreement with several studies, (e.g. Zhang and Delworth, 2005; Chiang and Bitz, 2005; Broccoli et al., 2006).

This has a direct impact on the precipitation near the Equator, with the southward shift of the main precipitation belt, by 10° or more, in the tropical Atlantic. The dipole pattern in the precipitation anomalies shown on Fig. 12 is located, in boreal winter,

with its negative anomaly centre at the Equator and positive anomaly centre at ca. 10° S, while in boreal summer this pattern is shifted North by ca. 10°. The anomaly pattern therefore follows the seasonal course of the main precipitation belt, which further proves the relationship between the shift in ITCZ and the tropical Atlantic precipitation anomalies. The comparison of the precipitation fields for LGMb and the corresponding LGMc–LGMb anomalies (Fig. 12, r.h.s and l.h.s, respectively) shows that the strong precipitation decrease off the Pacific coast of Central America can also be related to the southward shift of the ITCZ, although there is not as distinct a corresponding positive anomaly to the South, except in June–July–August (JJA). On the other hand, over the Amazon region, the increase in precipitation in September–October–November (SON) and December–January–February (DJF) is further amplified by a positive feedback involving increased evaporation (Fig. 14). Finally, the strong precipitation decrease over the Gulf of Mexico also appears to be associated with the southward shift of the ITCZ, or to an increase of the subsidence of the winter Hadley cell, since the anomalies are stronger in boreal autumn and winter and are not related to evaporation anomalies.

5.2 Impacts on monsoon systems, teleconnection between Indian region and North Atlantic

The impact of a strong weakening of the AMOC between the simulations LGMb and LGMc on the June to September (JJAS) precipitation is shown on Fig. 16a. The southward shift of the ITCZ in the Equatorial Atlantic is accompanied by a significant reduction in precipitation over the African monsoon region. Other modeling experiments (e.g. Chang et al., 2008) have highlighted the sensitivity of the African monsoon system to an additionnal fresh water flux in the North Atlantic and Arctic. In our experiments, this impact is verified under glacial conditions. However, there is no statistically significant change in JJAS precipitation over the East-Asian monsoon region, despite a decrease of the southerly monsoon winds over the China Sea (Fig. 16a).

The Indian monsoon precipitation is reduced by approximately 0.5 to 2 mm/day in the south-west of the subcontinent and in the northern Bay of Bengal. No changes are ob-

served over land since in the reference (LGMb) simulation, the largest monsoon signal is over the ocean. The reduction of the Indian monsoon intensity is also reflected in the weakened cross-equatorial flux from the Indian Ocean to the Arabian Sea (Fig. 16.a). Hence our modeling experiments additionally proves that a rather small freshwater flux anomaly (0.1 Sv) under glacial conditions can trigger a collapse of the AMOC and have a significant remote impact on the Indian summer monsoon activity. As stated in Sect. 1.1, this teleconnection has been investigated for different time scales (Gupta et al., 2003; Zhang and Delworth, 2005; Goswami et al., 2006; Lu et al., 2006; Feng and Hu, 2008). There are several pathways by which the monsoon rainfall may be influenced. The connection with the extratropics can find support in an atmospheric bridge with the changes over the North Atlantic. The influence of a weakening of the AMOC can also modify the (tropical) Walker circulation. Local ocean-atmosphere feedbacks, e.g. through changes in SSTs and evaporation, can amplify the changes.

A physical indicator of the Indian monsoon is based on the upper tropospheric temperature meridional gradient (Xavier et al., 2007; He et al., 2003). We have computed the average of tropospheric temperature from 200 to 500 hPa (TT) for the JJAS season. The difference of TT between the simulations LGMc and LGMb (Fig. 16b) indicates a significant seasonal cooling over the mid-latitudes. Over India, the meridional gradient of TT is reduced, as well as the sensitive heating over the Tibetan Plateau (not shown), resulting in weaker Indian monsoon precipitation. This mechanism is in agreement with the teleconnection observed between the Atlantic Multidecadal Oscillation and the Indian monsoon variability by Goswami et al. (2006) and Feng and Hu (2008). The anomaly of SSTs in the Northern Atlantic are passed in the upper troposphere over the whole Eurasian continent (cf. Sect. 4.2), creating an atmospheric bridge between the North Atlantic and the Asian region. Since the SST anomalies over the Indian Ocean and the Pacific are small, this mechanism appears to be predominant in these simulations. In addition, the evolution of the TT anomaly over the region (50°–100° E, 20°–50° N) and of the precipitation anomaly at the south-west of the peninsula is plotted on Fig. 16c. A 10 years boxcar smoothing is applied on the time series to remove

CPD
5, 1055–1107, 2009

the large interannual variability. The precipitation evolution follows that of TT anomalies and is stable after ca. 200 years. They are similar to the one of the maximum of AMOC (Fig. 1).

6 Summary and discussion

The present study analyses three glacial coupled atmosphere-ocean simulations characterised by different Atlantic Meridional Overturning Circulations (AMOC). In response to an 0.08 Sv increase in North Atlantic fresh water flux, the AMOC reduced from 18 Sv (LGMa) to 15 Sv (LGMb). The climate differences between these runs are restricted to the Northern North Atlantic, Nordic Seas and Europe. The cooling anomaly over the Northern North Atlantic associated to this slightly slower AMOC is strong enough to force a cyclonic anomaly in the atmospheric circulation over this region, which could take part in the slight warming over the Norwegian Sea. However, the main element explaining this surprising warm anomaly is the reinforcement of the convective activity in this area, partly resulting from the sea ice edge pushed further North by surface winds. A cooling anomaly appears further east in winter, due to northerly winds appearing as part of the stationary wave response to the SST changes over the North Atlantic and Nordic Seas. It is not possible to disentangle the roles of the atmosphere, ocean and sea ice in the temperature difference between the two simulations. Further tests, using partial coupling of the model components, would be needed to test if the atmospheric circulation changes and oceanic/sea ice response indeed seem to reinforce each other, especially over the Norwegian Sea, as suggested by our first analyses. The difference in precipitation, on the other hand, is hardly significant for these simulations.

A further 0.1 Sv fresh water flux into the North Atlantic induces a collapse of the AMOC in LGMc, compared to LGMb. The response to this shutdown does not appear to be a simple amplification of the climate anomalies simulated as a response to a weak AMOC perturbation. The surface climate anomalies are of global extent, and the analysis presented here focuses on three regions: the northern extratropi-

CPD
5, 1055–1107, 2009

cal response, the tropical Atlantic and the Indian monsoon. The climate response in the northern extratropics is dominated by large changes in stationary waves, with a strong cyclonic anomaly over the Northern North Atlantic persistent throughout the year, but stronger in winter and spring. These changes in stationary waves explain the smaller cooling over Western Europe, as compared to the North Atlantic, because this region is affected by southwesterly wind anomalies. They also explain a warming over the Northeastern Pacific and America's northwestern coast, affected by southwesterly wind anomalies too. The precipitation anomalies over the Atlantic extratropics are mostly related to a strong evaporation decrease due to the cooling there and not so much to amospheric circulation changes, such as in other regions. Indeed, over the Northeastern Pacific/Northwestern America, for example, they appear to be also related with a southward shift of the westerlies/storm-tracks.

The collapse of the AMOC is accompanied by a decrease in meridional oceanic heat transport, strongest in the Atlantic basin, and only partly compensated by an increase of the transport in the other ocean basins and by an increase in atmospheric heat transport. The atmospheric meridional heat transport increase occurs via an adjustment of the meridional circulation, and most notably of the Hadley cells. The structure of the atmospheric meridional circulation shifts southward by around 10° in the Tropics. This is accompanied by a dipole in the precipitation anomalies, with a drying north of the thermal equator and a wettening south of it, which constitutes the hydrological signature of the southward shift of the ITCZ. This signature is most prominent in the tropical Atlantic, but part of the precipitation anomalies in the eastern tropical Pacific can also be ascribed to this mechanism. The increase in precipitation over the Amazon region appears to be amplified by a local evaporation-precipitation feedback. Finally, we analyse the weakening of the Indian monsoon in response to the AMOC collapse as a consequence of an atmospheric bridge between the North Atlantic and the monsoon area, which involves the large cooling of the upper tropospheric over Eurasia, and the subsequent decrease in the tropospheric meridional gradient between India and Northern Eurasia. These surface climate changes associated to an AMOC shutdown do not

CPD
5, 1055–1107, 2009

appear simultaneously in all reagions of the globe. The timing of the response is of the order of a hundred years over the Atlantic, Eurasia and for the Indian monsoon. The response over the northwestern Pacific is the slowest to appear, with a timescale of around 250 years. Over the tropical Atlantic, the response at intermediate timescales, hence highlighting fast atmospheric adjustements and slower ocean related features, characterised by the advection of anomalies (in particular in temperatures) in the sub-tropical gyre.

The hydrological cycle is deeply affected by a collapse in the AMOC and one can wonder whether this constitutes a positive or a negative feedback compared to the freshwater anomaly which is the initial cause of the AMOC collapse. The freshwater budget (precipitation plus runoff minus evaporation) over the Atlantic for the years 370 to 420 is shown on Fig. 17. The calving perturbation anomaly summed for the North Atlantic north of 40° N amounts to 104 mSv in LGMc compared to LGMb. In the same region, the net freshwater anomalies amounts to 79 mSv after 420 years in LGMc compared to LGMb. This reduction is therefore smaller than the calving flux perturbation (104 mSv). This reduction in the perturbation is due to a decrease in precipitation there, which is not totally compensated by the decrease in evaporation associated with the cooling in this region. In remote areas, where no calving perturbation is applied, important freshwater anomalies are found. From 15° N to 40° N, a positive freshwater anomaly of 56 mSv is simulated, mainly due to a large decrease in evaporation in this latitudinal band (Fig. 17). The southward shift of the ITCZ affects the equatorial region in the Atlantic so that a 119 mSv negative freshwater anomaly is found from 4° N to 15° N and a 191 mSv positive freshwater anomaly is found from 10° S to 4° N. On the whole Atlantic (north of 30° S), the freshwater anomalies amount to 185 mSv, including the 104 mSv for the calving freshwater perturbation, representing an 81 mSv additional increase in the global Atlantic freshwater input.

The southward shift of the ITCZ is therefore associated with a net change in the freshwater fluxes around the Equator. Leduc et al. (2007) suggest that a southward shift in the ITCZ will diminish the westward export of freshwater in the atmosphere

CPD
5, 1055–1107, 2009

through Central America because of the orogenic blocking of moisture transport by the Andes. Freshwater would then return to the Atlantic, notably through the Amazon Basin drainage, which could act as a positive feedback on the AMOC reduction if this fresh water anomaly reached in North Atlantic. This effect appears clearly here in the peak in runoff anomaly found around the Equator (Fig. 17). Nonetheless, the freshwater budget for the North Atlantic north of 4° N is negative (−90 mSv when the calving perturbation is deduced). This region includes the convection sites and encompasses both the northern subtropical and subpolar gyres that exchange large amounts of fresh water, which can strongly affect the density of the convection sites. The freshwater changes over this region are likely to be more important than those over the tropical Atlantic region south of 4° N, so that eventually, the changes in freshwater budget in response to the AMOC collapse will tend to increase the salinity in the convection sites. Thus, we argue in line with dedicated sensitivity analysis (Krebs and Timmermann, 2007) that the freshwater response to AMOC changes is more likely a negative feedback. This would have to be confirmed via complementary, partially coupled, sensitivity experiments.

In this work, we have focused our analyses on three regions: the northern extratropics, the tropical Atlantic and the Indian monsoon area. These are regions where the sensitivity of our climate model to a collapse in AMOC is strongest and broadly consistent with paleo-records. There are other regions for which our model does not show as large a response as suggested by data. For instance, East Antarctica and the East Asian monsoon areas do not undergo large changes in temperature or precipitation. This could be related to a lack of sensitivity of the model used, to missing feedbacks (from the dust or biogeochemical cycles, for instance) or to the chosen LGM basic state. Indeed the largest glacial climatic variations are recorded during Marine Isotopic Stage 3, during which the ice-sheet size and atmospheric greenhouse gas concentrations are intermediate between the interglacial and LGM states. It would therefore be interesting to compare our results to results from other models and to similar experiments, but with smaller ice-sheets and/or different greenhouse gas concentrations/insolation.

Acknowledgements. All simulations presented in this work were run on the Commissariat l'Energie Atomique super-computing facilities. This study has been partly funded by ANR-BLANC IDEGLACE (ANR-05-BLAN-0310-01).

The publication of this article is financed by CNRS-INSU.

References

Alkama, R., Kageyama, M., Ramstein, G., Marti, O., Ribstein, P., and Swingedouw, D.: Impact of a realistic river routing in coupled oceanatmosphere simulations of the Last Glacial Maximum climate, Clim. Dynam., 30, 855–869, 2008. 1065, 1072

Altabet, M. A., Higginson, M. J., and Murray, D. W.: The effect of millennial-scale changes in Arabian Sea denitrification on atmospheric CO2, Nature, 415, 159–162, 2002. 1060

Berger, A. L.: Long-term variations of daily insolation and Quaternary climatic changes, J. Atmos. Sci., 35, 2362–2367, 1978. 1065

Bjerknes, J.: Atlantic air-sea interaction, Academic Press, 10, 1–82, 1964. 1067

Blunier, T., Chappellaz, J., Schwander, J., Dällenbach, A., Stauffer, B., Stocker, T. F., Raynaud, D., Jouzel, J., Clausen, H. B., Hammer, C. U., and Johnsen, S. J.: Asynchrony of Antarctic and Greenland climate change during the last glacial period, Nature, 394, 739–743, 1998. 1057, 1060

Bond, G., Broecker, W., Johnsen, S., McManus, J., Labeyrie, L., Jouzel, J., and Bonani, G.: correlations between climate records from North Atlantic sediments and Greenland ice, Nature, 365, 143–147, 1993. 1057

Bout-Roumazeilles, V., Nebout, N. C., Peyron, O., Cortijo, E., Landais, A., and Masson-Delmotte, V.: Connection between South Mediterranean climate and North African atmo-

spheric circulation during the last 50,000 yr BP North Atlantic cold events, Quaternary Sci. Rev., 26, 3197–3215, 2007. 1058
Braconnot, P., Otto-Bliesner, B., Harrison, S., Joussaume, S., Peterchmitt, J.-Y., Abe-Ouchi, A., Crucifix, M., Driesschaert, E., Fichefet, Th., Hewitt, C. D., Kageyama, M., Kitoh, A., Laîné, A., Loutre, M.-F., Marti, O., Merkel, U., Ramstein, G., Valdes, P., Weber, S. L., Yu, Y., and Zhao, Y.: Results of PMIP2 coupled simulations of the Mid-Holocene and Last Glacial Maximum - Part 1: experiments and large-scale features, Clim. Past, 3, 261–277, 2007, http://www.clim-past.net/3/261/2007/. 1065
Broccoli, A. J., Dahl, K. A., and Stouffer, R. J.: Response of the ITCZ to Northern Hemisphere cooling, Geophys. Res. Lett., 33, L01702, doi:10.1029/2005GL024546, 2006. 1077
Chang, P., Zhang, R., Hazeleger, W., Wen, C., Wan, X. Q., Ji, L., Haarsma, R. J., Breugem, W. P., and Seidel, H.: Oceanic link between abrupt changes in the North Atlantic Ocean and the African monsoon, Nature Geoscience, 1, 444–448, 2008. 1078
Chiang, J. C. H. and Bitz, C. M.: Influence of high latitude ice cover on the marine Intertropical Convergence Zone, Clim.e Dynam., 25, 477–496, 2005. 1062, 1077
Chiang, J. C. H., Cheng, W., and Bitz, C. M.: Fast teleconnections to the tropical Atlantic sector from Atlantic thermohaline adjustment, Geophys. Res. Lett., 35, L07704, doi:10.1029/2008GL033292, 2008. 1062
Claussen, M., Ganopolski, A., Brovkin, V., Gerstengarbe, F.-W., and Werner, P.: Simulated global-scale response of the climate system to Dansgaard/Oeschger and Heinrich events, Clim. Dynam., 21, 361–370, 2003. 1063
Combourieu Nebout, N., Turon, J.-L., Zhan, R., Capotondi, L., Londeix, L., and Pahnke, K.: Enhanced aridity and atmospheric high-pressure stablity over the western Mediterranean during the North Atlantic cold events of the past 50 k.y., Geology, 30, 863–866, 2002. 1058
Dallenbach, A., Blunier, T., Fluckiger, J., Stauffer, B., Chappellaz, J., and Raynaud, D.: Changes in the atmospheric CH_4 gradient between Greenland and Antarctica during the Last Glacial and the transition to the Holocene, Geophys. Res. Lett., 27, 1005–1008, 2000. 1065
Dansgaard, W., Johnsen, S. J., Clausen, H. B., Dahl-Jensen, D., Gundestrup, N. S., Hammer, C. U., Hvidberg, C. S., Steffensen, J. P., Sveinbjörnsdottir, A. E., Jouzel, J., and Bond, G.: Evidence for general instability of past climate from a 250-kyr ice-core record, Nature, 364, 218–220, 1993. 1057
Denton, G. H., Alley, R. B., Comer, G. C., and Broecker, W. S.: The role of seasonality in abrupt climate change, Quaternary Sci. Rev.s, 24, 1159–1182, 2005. 1059, 1074

Elliot, M., Labeyrie, L., and Duplessy, J.-C.: Changes in North Atlantic deep-water formation associated with the Dansgaard-Oeschger temperature oscillations (60–10 ka), Quaternary Sci. Rev., 21, 1153–1165, 2002. 1057

EPICA community members: One-to-one coupling of glacial climate variability in Greenland and Antarctica, Nature, 444, 195–198, 2006. 1057, 1060

Feng, S. and Hu, Q.: How the North Atlantic Multidecadal Oscillation may have influenced the Indian summer monsoon during the past two millennia, Geophys. Res. Lett., 35, L01707, doi:10.1029/2007GL032484, 2008. 1079

Flückiger, J., Dällenbach, A., Blunier, T., Stauffer, B., Stocker, T. F., Raynaud, D., and Barnola, J.-M.: Variations in atmospheric N_2O concentration during abrupt climatic changes, Science, 285, 227–230, 1999. 1065

Flückiger, J.,Knutti, R., White, J. W. C., and Renssen, H.: Modeled seasonality of glacial abrupt climate events, Clim. Dynam., 31, 633–645, 2008. 1064

Ganopolski, A. and Rahmstorf, S.: Rapid changes of glacial climate simulated in a coupled climate model, Nature, 409, 153–158, 2001. 1063

Genty, D., Blamart, D., Ouahdi, R., Gilmour, M., Baker, A., Jouzel, J., and Van-Exter, S.: Precise dating of Dansgaard-Oeschger climate oscillations in western Europe from stalagmite data, Nature, 421, 833–937, 2003. 1058

González, C., Dupont, L. M., Behling, H., and Wefer, G.: Neotropical vegetation response to rapid climate changes during the last glacial period: Palynological evidence from the Cariaco Basin, Quaternary Res., 69, 217–230, 2008. 1059

Goswami, B. N., Madhusoodanan, M. S., Neema, C. P., and Sengupta, D.: A physical mechanism for North Atlantic SST influence on the Indian summer monsoon, Geophys. Res. Lett., 33, L02706, doi:10.1029/2005GL024803, 2006. 1062, 1079

Grimm, E. C., Watts, W. A., Jacobson Jr., G. L., Hansen, B. C. S., Almquist, H. R., and Dieffenbacher-Krall, A. C.: Evidence for warm wet Heinrich events in Florida, Quaternary Sci. Rev., 25, 2197–2211, 2006. 1058

Gupta, A. K., Anderson, D. M., and Overpeck, J. T.: Abrupt changes in the Asian southwest monsoon during the Holocene and their links to the North Atlantic Ocean, Nature, 421, 354–357, 2003. 1079

He, H. Y., Sui, C. H., Jian, M. Q., Wen, Z. P., and Lan, G. D.: The evolution of tropospheric temperature field and its relationship with the onset of Asian summer monsoon, J. Meteorol. Soc. Jpn., 81, 1201–1223, 2003. 1079

Heinrich, H.: Origin and consequences of cyclic ice rafting in the Northeast Atlantic ocean during the past 130 000 years, Quaternary Res., 29, 142–152, 1988. 1057
Hewitt, C. D., Broccoli, A. J., Crucifix, M., Gregory, J. M., Mitchell, J. F. B., and Stouffer, R. J.: The effect of a large freshwater perturbation on the glacial North Atlantic ocean using a coupled General Circulation Model, J. Climate, 19, 4436–4447, 2006. 1063
Hu, A., Otto-Bliesner, B. L., Meehl, G. A., Han, W., Morrill, C., Brady, E. C., and Briegleb, B.: Response of Thermohaline Circulation to Freshwater Forcing under Present Day and LGM Conditions, J. Climate, 21, 2239–2258, 2008. 1063
Jin, L., Chen, F., Ganopolski, A., and Claussen, M.: Response of East Asian climate to Dansgaard-Oeschger and Heinrich events in a coupled model of intermediate complexity, J. Geophys. Res., 112, D06117, doi:10.1029/2006JD007316, 2007. 1063
Jullien, E., Grousset, F., Malaize, B., Duprat, J., Sanchez-Goni, M. F., Eynaud, F., Charlier, K., Schneider, R., Bory, A., Bout, V., and Flores, J. A.: Low-latitude "dusty events" vs. high-latitude "icy Heinrich events", Quaternary Res., 68, 379–386, 2007. 1059
Kissel, C.: Magnetic signature of rapid climatic variations in glacial North Atlantic, a review, C.R. Geosci., 337, 908–918, 2005. 1057
Krebs, U. and Timmermann, A.: Tropical air-sea interactions accelerate the recovery of the Atlantic Meridional Overturning Circulation after a major shutdown, J. Climate, 20, 4940–4956, 2007. 1063, 1083
Leduc, G., Vidal, L., Tachikawa, K., Rostek, F., Sonzogni, C., Beaufort, L., and Bard, E.: Moisture transport across Central America as a positive feedback on abrupt climatic changes, Nature, 445, 908–911, 2007. 1059, 1082
Leuschner, D. C. and Sirocko, F.: The low-latitude monsoon climate during Dansgaard-Oeschger cycles and Heinrich Events, Quaternary Sci. Rev., 19, 243–254, 2000. 1060
Lu, R., Dong, B., and Ding, H.: Impact of the Atlantic Multidecadal Oscillation on the Asian summer monsoon, Geophys. Res. Lett., 33, L24701, doi:10.1029/2006GL027655, 2006. 1062, 1079
Manabe, S. and Stouffer, R. J.: Simulation of abrupt climate change induced by freshwater input to the North Atlantic Ocean, Nature, 378, 165–167, 1995. 1060
Marti, O., Braconnot, P., Bellier, J., Benshila, R., Bony, S., Brockmann, P., Cadule, P., Caubel, A., Denvil, S., Dufresne, J.-L., Fairhead, L., Filiberti, M.-A., Foujols, M.-A., Fichefet, T., Friedlingstein, P., Goosse, H., Grandpeix, J.-Y., Hourdin, F., Krinner, G., Lévy, C., Madec, G., Musat, I., de Noblet, N., Polcher, J., and Talandier, C.: The new IPSL climate system

model: IPSL-CM4, Tech. Rep. 26, IPSL, Note du Pôle de Modélisation, ISSN 1288-1619, 84 pp., 2006. 1065

Marti, O., Braconnot, P., Dufresne, J.-L., Hourdin, F., Denvil, S., Friedlingstein, P., Swingedouw, D., Mignot, J., Goosse, H., Fichefet, T., Codron, F., Guilyardi, E., Bellier, J., Benshila, R., Bony, S., Brockmann, P., Cadule, P., Caubel, A., Fairhead, L., Foujols, M.-A., Grandpeix, J.-Y., Hourdin, F., Kageyama, M., Krinner, G., Lvy, C., Madec, G., Musat, I., de Noblet, N., and Talandier, C.: Key features of the IPSL ocean atmosphere model and its sensitivity to atmospheric resolution, Clim. Dynam., in revision, 2008. 1065

Monnin, E., Indermuhle, A., Dallenbach, A., Fluckiger, J., Stauffer, B., Stocker, T. F., Raynaud, D., and Barnola, J.-M.: Atmospheric CO_2 concentrations over the last glacial termination, Science, 291, 112–114, 2001. 1065

Muller, J., Kylander, M., Wüst, R. A. J., Weiss, D., Martinez-Cortizas, A., LeGrande, A. N., Jennerjahn, T., Behling, H., Anderson, W. T., and Jacobson, G.: Possible evidence for wet Heinrich phases in tropical NE Australia: the Lynchs Crater deposit, Quaternary Sci. Rev., 27, 468–475, 2008. 1059

Peltier, W. R.: GLOBAL GLACIAL ISOSTASY AND THE SURFACE OF THE ICE-AGE EARTH: The ICE-5G (VM2) Model and GRACE, Annu. Revi. Earth Pl. Sc., 32, 111–149, 2004. 1065

Peterson, L. C., Haug, G. H., Hughen, K. A., and Röhl, U.: Rapid changes in the hydrologic cycle of the tropical North Atlantic during the last glacial, Science, 290, 1947–1951, 2000. 1059

Porter, S. and An, Z.: Correlation between climate events in the North Atlantic and China during the last glaciation, Nature, 375, 305–308, 1995. 1059

Rahmstorf, S.: Rapid climate transitions in a coupled ocean-atmosphere model, Nature, 372, 82–85, 1994. 1060

Rashid, H., Flower, B. P., Poore, R. Z., and Quinn, T. M.: A similar to 25 ka Indian Ocean monsoon variability record from the Andaman Sea, Quaternary Sci. Rev., 26, 2586–2597, 2007. 1060

Ruth, U., Bigler, M., Röthlisberger, R., Siggard-Andersen, M.-L., Kipfstuhl, S., Goto-Azuma, K., Hansson, M. E., Johnsen, S. J., Lu, H., and Steffensen, J. P.: Ice core evidence for a very tight link between North Atlantic and east Asian glacial climate, Geophys. Res. Lett., 34, L03706, doi:10.1029/2006GL027876, 2007. 1059

Saenko, O. A., Weaver, A. J., Robitaille, D. Y., and Flato, G. M.: Warming of the subpolar Atlantic triggered by freshwater discharge at the continental boundary, Geophys. Res. Lett.,

34, L15604, doi:10.1029/2007GL030674, 2007. 1061
Sánchez-Goñi, M. F., Landais, A., Fletcher, W. J., Naughton, F., Desprat, S., and Duprat, J.: Contrasting impacts of Dansgaard-Oeschger events over a western European latitudinal transect modulated by orbital parameters, Quaternary Sci. Rev., 27, 1136–1151, 2008. 1058, 1060
Sánchez-Goñi, M.-F., Cacho, I., Turon, J.-L., Guiot, J., Sierro, F. J., Peypouquet, J.-P., Grimalt, J. O., and Shackleton, N. J.: Synchroneity between marine and terrestrial responses to millennial scale climatic cariability during the last glacial period in the Mediterranean region, Clim. Dynam., 19, 95–105, 2002. 1058
Schulz, H., von Rad, U., and Erlenkeuser, H.: Correlation between Arabian Sea and Greenland climate oscillations of the past 110 000 years, Nature, 393, 54–57, 1998. 1060
Shaffrey, L. and Sutton, R.: Bjerknes compensation and the decadal variability of the energy transports in a coupled climate model, J. Climate, 19, 1167–1181, 2006. 1067, 1070
Stocker, T. F.: Climate change – The seesaw effect, Science, 282, 61–62, 1998. 1062
Stommel, H. M.: Thermohaline convection with two stable regimes of flow, Tellus, 13, 224–230, 1961. 1060
Stouffer, R. J., Yin, J., Gregory, J. M., Diwon, K. W., Spelman, M. J., Hurlin, W., Weaver, A. J., Eby, M., Flato, G. M., Hasumi, H., Hu, A., Jungclaus, J. H., Kamenovich, I. V., Levermann, A., Montoya, M., Murakami, S., Nawrath, S., Oka, A., Peltier, W. R., Robitaille, D. Y., Sokolov, A., Vettoretti, G., and Weber, S. L.: Investigating the causes of the response of the thermohaline circulation to past and future climate changes, J. Climate, 19, 1365–1387, 2006. 1060, 1061, 1067
Swingedouw, D., Mignot, J., Braconnot, P., Mosquet, E., Kageyama, M., and Alkama, R.: Impact of freshwater release in the North Atlantic under different climate conditions in an OAGCM, J. Climate, submitted, 2008. 1069
Timmermann, A., Krebs, U., Justino, F., Goosse, H., and Ivanochko, T.: Mechanisms for millennial-scale global synchronization during the last glacial period, Paleoceanography, 20, PA4008, doi:10.1029/2004PA001090, 2005. 1063
Turney, C. S. M., Kershaw, A. P., Clemens, S. C., Branch, N., Moss, P. T., and Fifield, L. K.: Millennial and orbital variations of El Niño/Southern Oscillation and high-latitude climate in the last glacial period, Nature, 428, 306–310, 2004. 1059
Vellinga, M. and Wood, R. A.: Global climatic impacts of a collapse of the Atlantic thermohaline circulation, Climatic Change, 54, 251–267, 2002. 1061

Wang, X., Auler, A. S., Edwards, R. L., Cheng, H., Cristalli, P. S., Smart, P. L., Richards, D. A., and Shen, C.-C.: Wet periods in northeastern Brazil over the past 210 kyr linked to distant climate anomalies, Nature, 432, 740–743, 2004. 1059

Wang, Y. J., Cheng, H., Edwards, R. L., An, Z. S., Wu, J. Y., Shen, C.-C., and Dorale, J. A.: A high-resolution absolute-dated late Pleistocene monsoon record from Hulu Cave, China, Science, 294, 2345–2348, 2001. 1059

Winton, M.: On the climatic impact of ocean circulation, J. Climate, 16, 2875–2889, 2003. 1068

Xavier, P. K., Marzin, C., and Goswami, B. N.: An objective definition of the Indian summer monsoon season and a new perspective on the ENSO-monsoon relationship, Q. J. Roy. Meteor. Soc., 133, 749–764, 2007. 1079

Yang, H. and Liu, Z.: Tropical-extra-tropical climate interaction as revealed in idealized coupled climate model experiments, Clim. Dynam., 24, 863–879, 2005. 1062, 1070

Zhang, R. and Delworth, T. L.: Simulated tropical response to a substantial weakening of the Atlantic thermohaline circulation, J. Climate, 18, 1853–1860, 2005. 1062, 1077, 1079

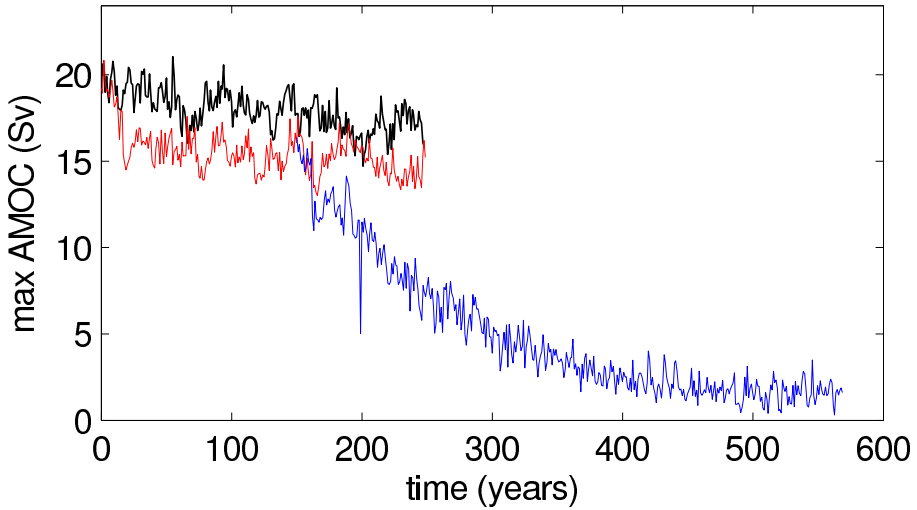

Fig. 1. Time evolution of the Maximum of the Atlantic Meridional Overturning Circulation (in Sv) in runs LGMa (black), b (red) and c (blue).

CPD

5, 1055–1107, 2009

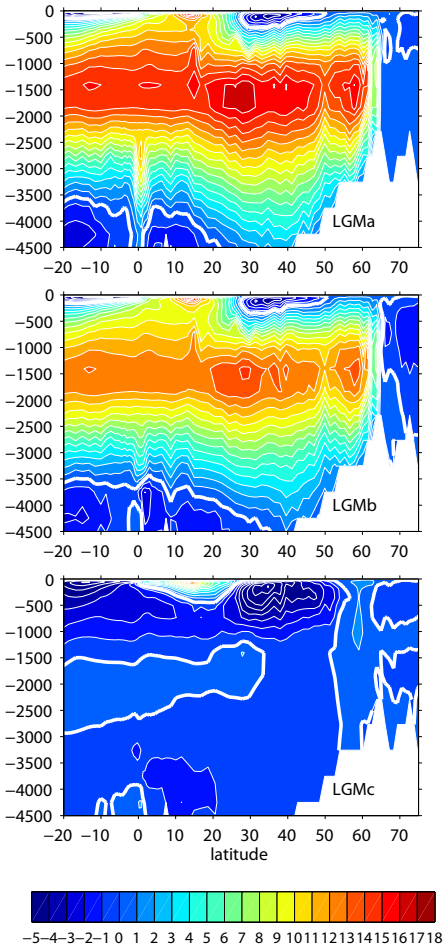

Fig. 2. Atlantic Meridional Streamfunction for LGMa (top), LGMb (middle), LGMc (bottom), years 201–250 for LGMa and b, 371–420 for LGMc. Contour interval: 1 Sv (1 Sv=10^6 m^3/s).

CPD
5, 1055–1107, 2009

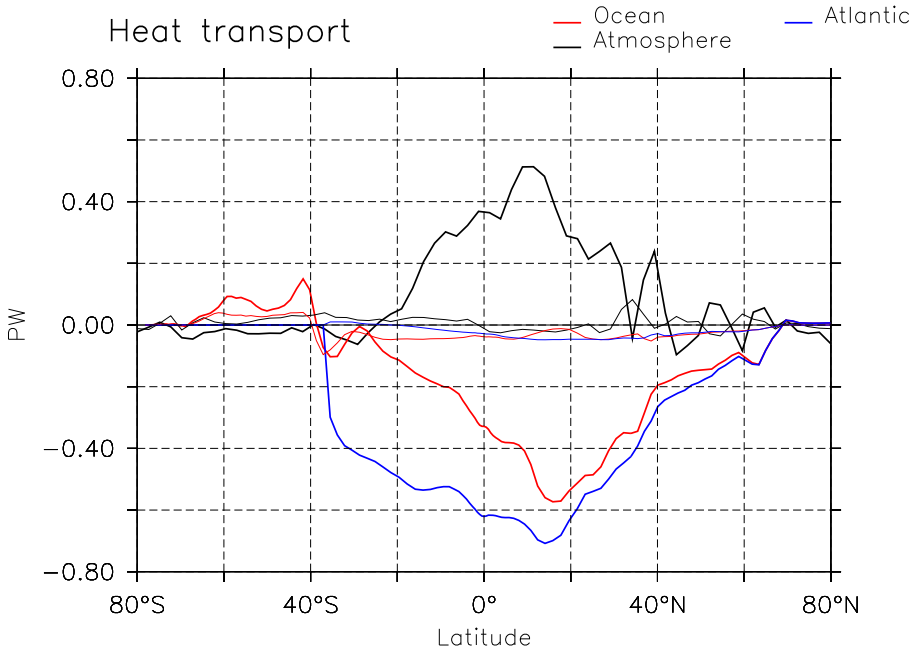

Fig. 3. Difference in zonally averaged meridional heat transports (in PW), between LGMa and LGMb (thin lines) and between LGMc and LGMb (thick lines). In red: the oceanic heat transport difference, in black: the atmospheric heat transport difference and in blue: the Atlantic heat transport difference. The time averages are taken over years 201–250 for LGMa and LGMb, and over years 371–420 for LGMc.

CPD
5, 1055–1107, 2009

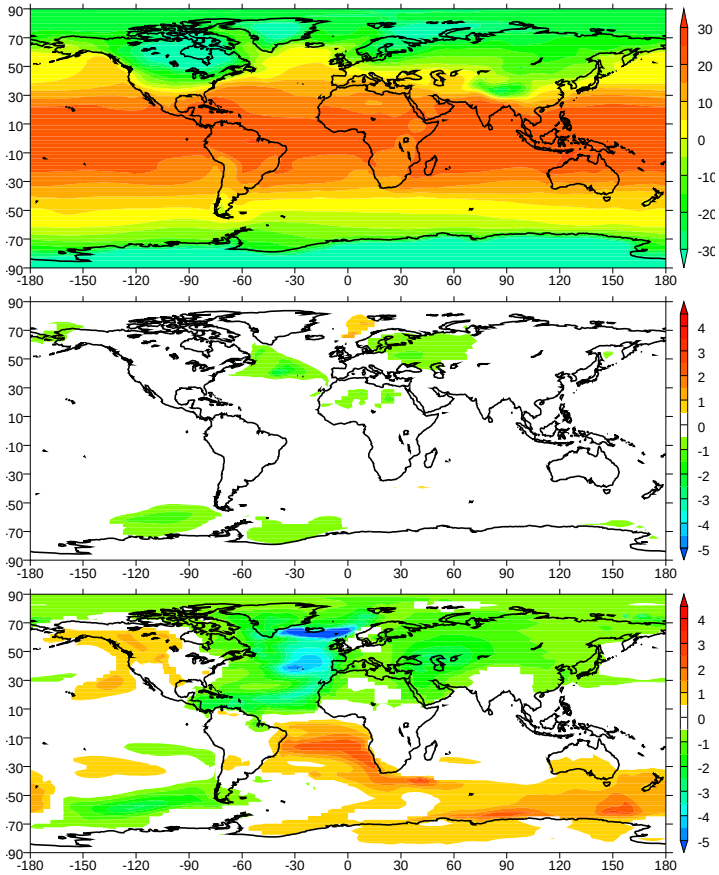

Fig. 4. Mean annual temperature (˚C). Top: LGMa; middle: LGMb−LGMa; bottom: LGMc–LGMb. The differences have been masked where not significant at the 95% level in a standard Student-T test. The time averages are taken over years 201–250 for LGMa and LGMb, and over years 371–420 for LGMc.

CPD
5, 1055–1107, 2009

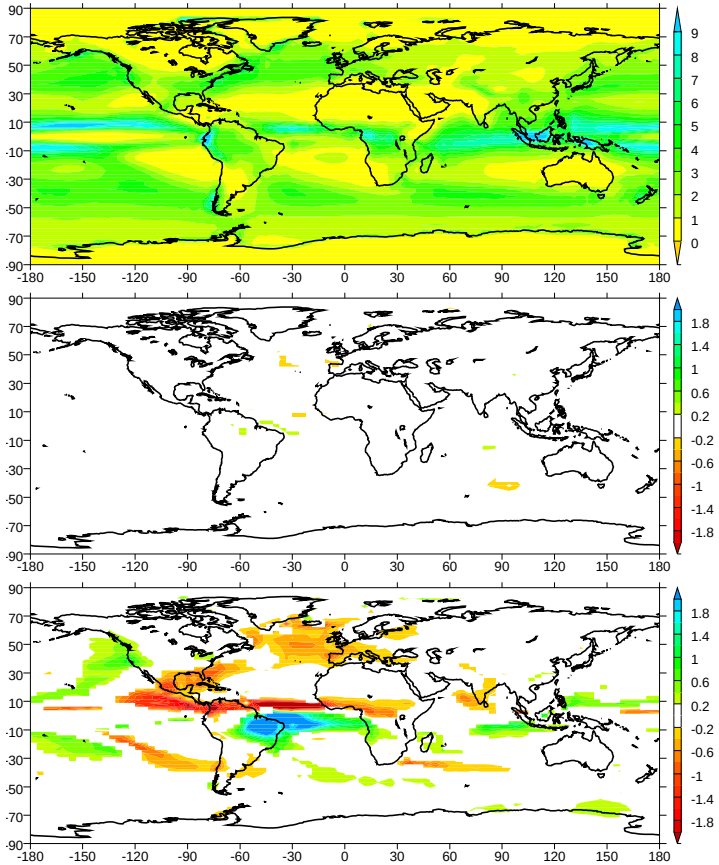

Fig. 5. Mean annual precipitation (mm/day). Top: LGMa; middle: LGMb–LGMa; bottom: LGMc–LGMb. The differences have been masked where not significant at the 95% level in a standard Student-T test. The time averages are taken over years 201–250 for LGMa and LGMb, and over years 371–420 for LGMc.

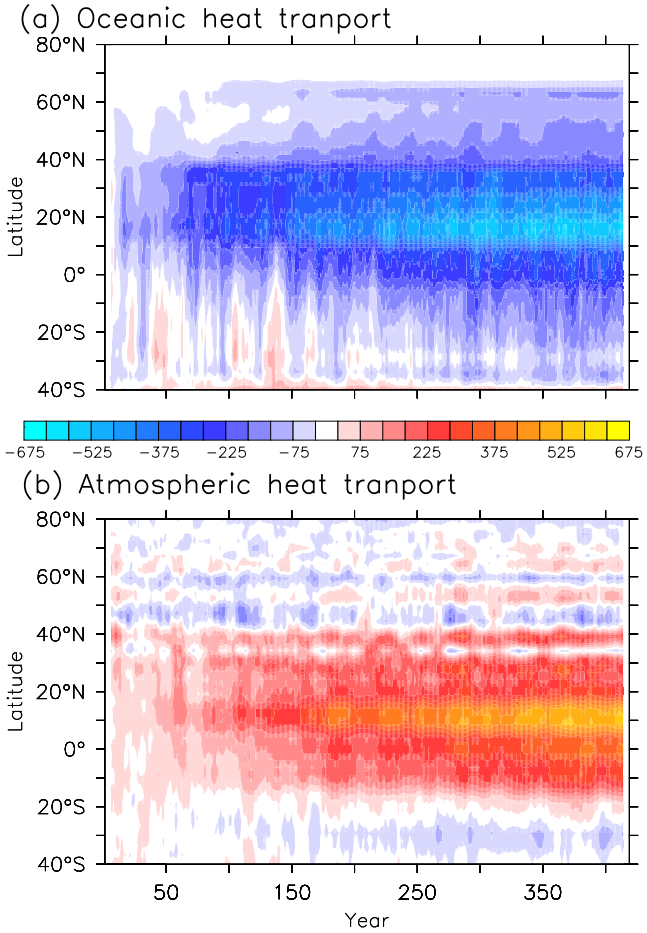

Fig. 6. Difference (LGMc–LGMb) in meridional heat transport in latitude-time space, averaged zonally on **(a)** the global ocean and **(b)** the global atmosphere. The contour interval is 50 TW.

CPD
5, 1055–1107, 2009

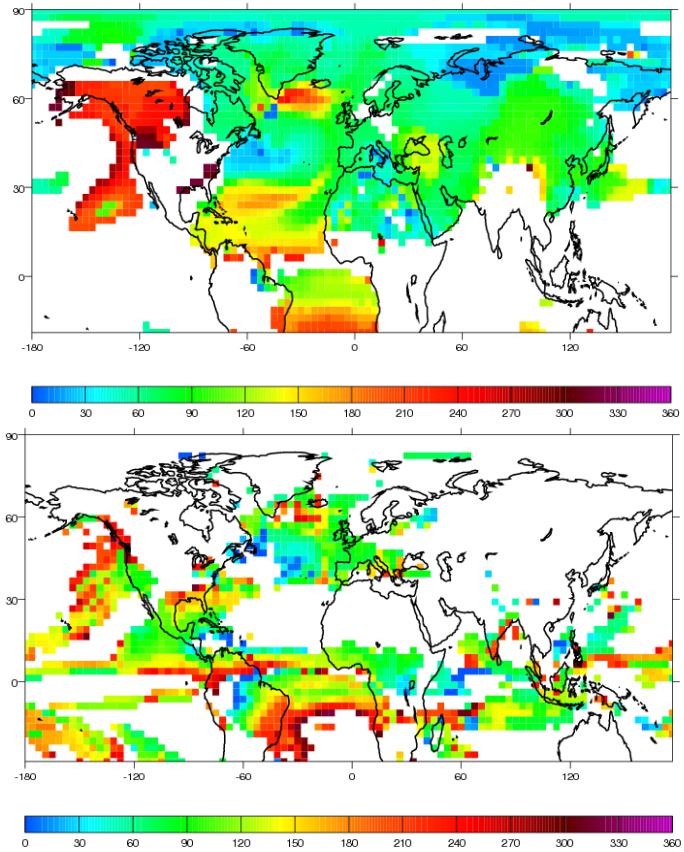

Fig. 7. Top: Timing of the appearance of significant anomalies in mean annual temperature in LGMc, as compared to LGMb, defined as the first year in which the anomaly reaches at least half of the final anomaly for at least 50 years (the "final" anomaly is taken as the difference between years 371–420 of LGMc and years 100–150 of LGMb). Bottom: Same as for top but for the mean annual precipitation (cf. final response Fig. 5).

CPD
5, 1055–1107, 2009

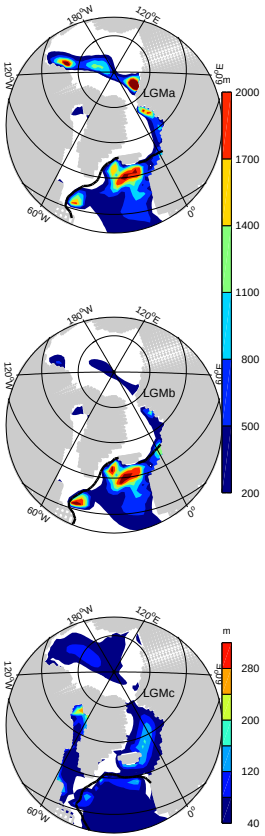

Fig. 8. Maximum mixed layer depth reached over the winter months February to April. Top: LGMa, middle: LGMb, bottom: LGMc. The thick black line shows the limit of a 10% sea ice coverage in March. The time averages are taken over years 201–250 for LGMa and LGMb, and over years 371–420 for LGMc. Contour interval: 40 m.

CPD
5, 1055–1107, 2009

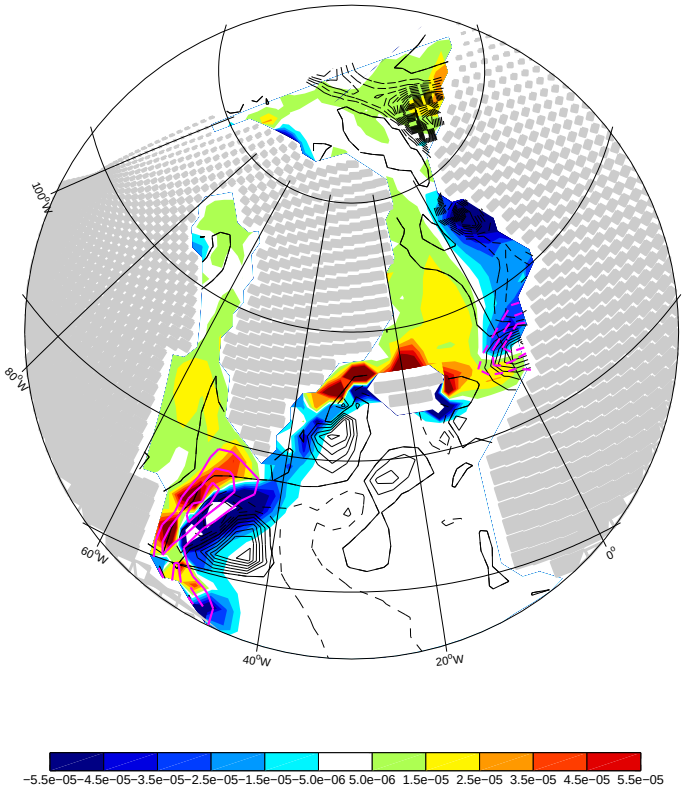

Fig. 9. Colors: ice to ocean winter (JFM) anomalous (LGMb-LGMa) freshwater budget (in kg/m^2/s). black contours: anomalous (LGMb-LGMa) winter (JFM) mixed layer depth. Continuous (dashed) contours show positive (negative) anomalies. Contour interval is 100 m. The contour of zero anomaly is omitted. Pink contours: anomalous (LGMb-LGMa) winter (JFM) ice coverage. Continuous (dashed) contours show positive (negative) anomalies. Contour interval: 0.1 kg/m^2/s.

CPD
5, 1055–1107, 2009

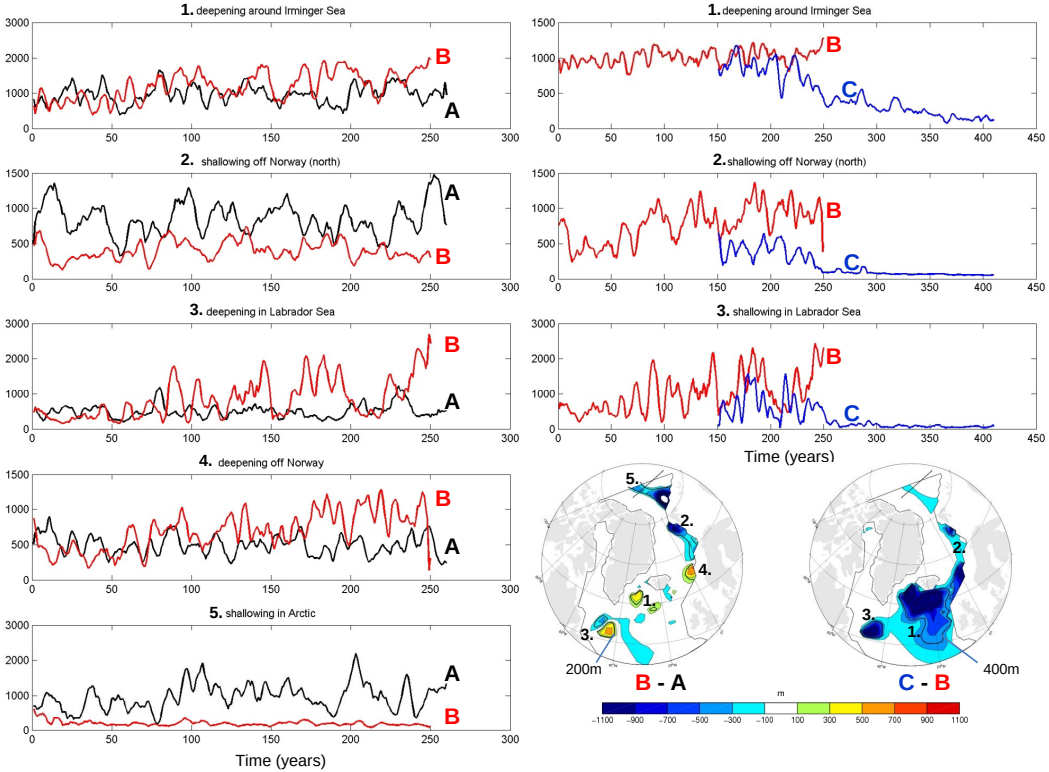

Fig. 10. Timeseries of winter mean mixed layer depth (m) averaged over areas of anomalous deep convection (indicated on the maps below the time series). Black line: LGMa, red line: LGMb, blue line: LGMc. All annual time series have been low-passed filtered using a 5-point running mean.

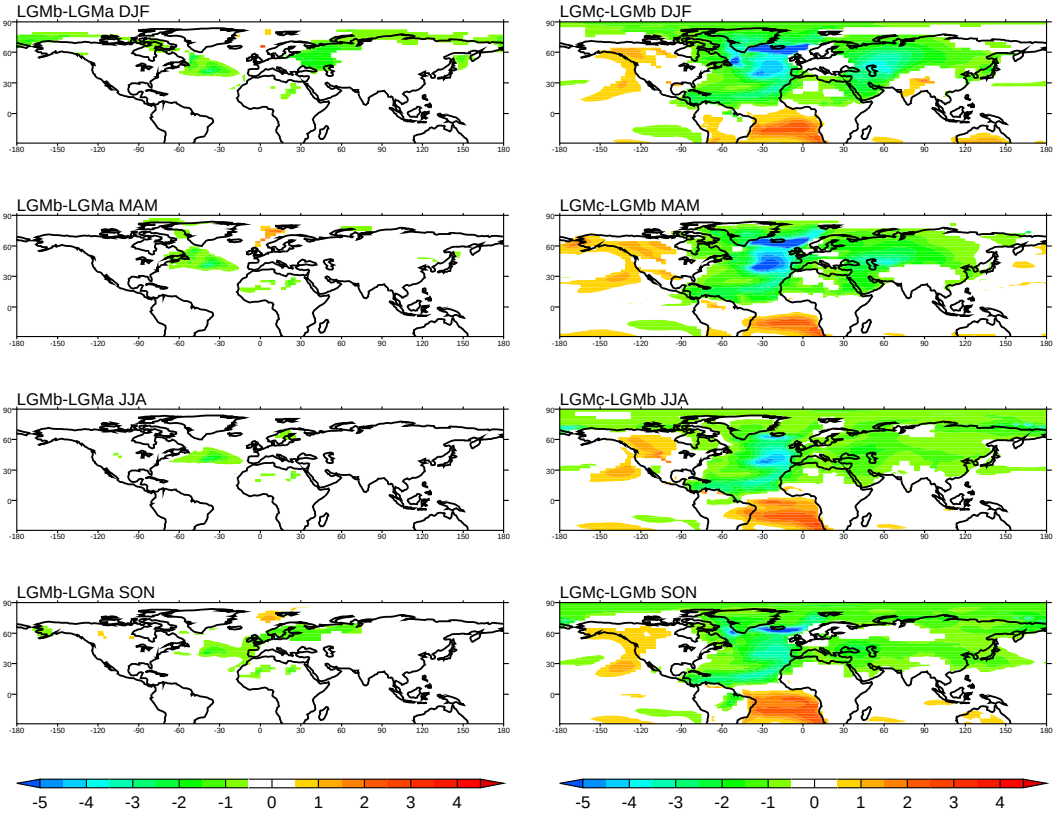

Fig. 11. LGMb–LGMa anomalies (l.h.s.) and LGMc–LGMb anomalies (r.h.s) in 2 m temperatures (in °C) for the 4seasons. The differences have been masked where not significant at the 95% level in a standard Student-T test. The time averages are taken over years 201–250 for LGMa and LGMb, and over years 371–420 for LGMc.

CPD
5, 1055–1107, 2009

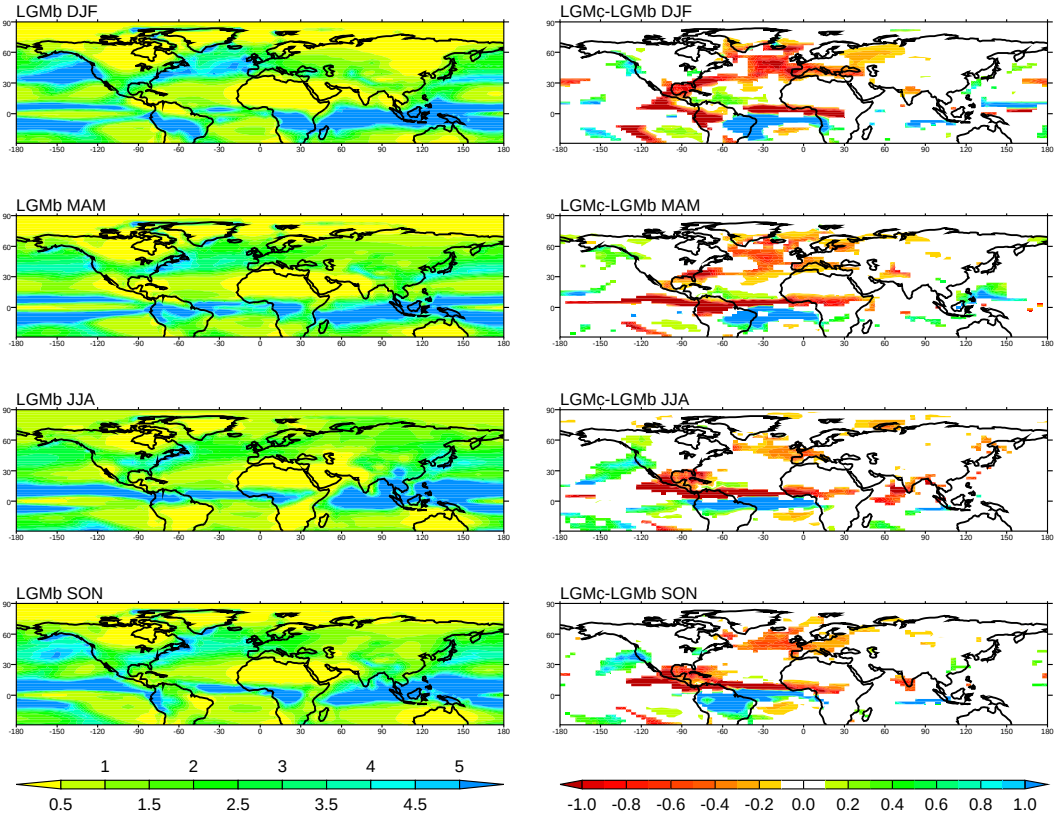

Fig. 12. LGMb precipitation (l.h.s.) and LGMc–LGMb precipitation anomalies (r.h.s) in mm/day for the 4 seasons. The differences have been masked where not significant at the 95% level in a standard Student-T test. The time averages are taken over years 201–250 for LGMb and over years 371–420 for LGMc.

CPD
5, 1055–1107, 2009

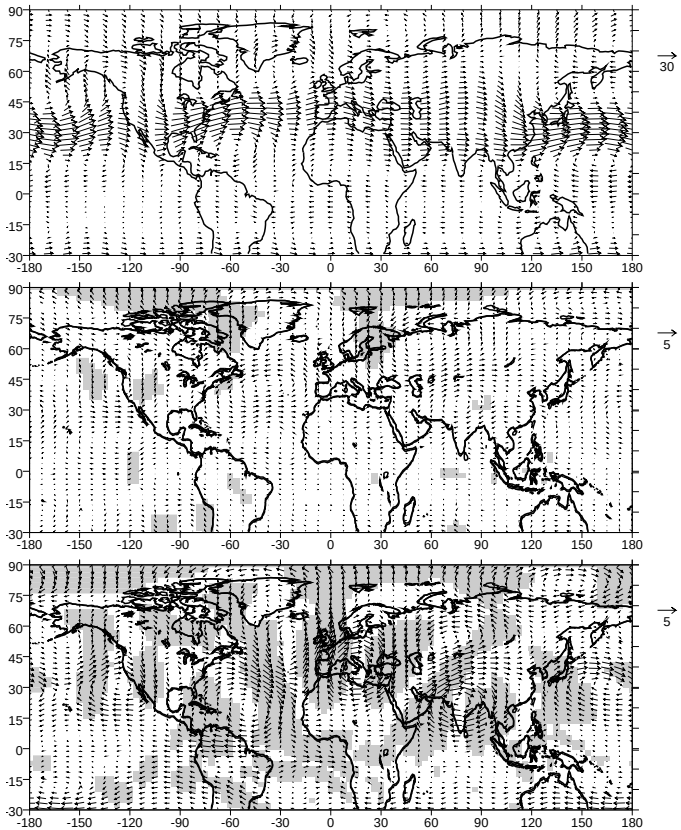

Fig. 13. 500 hPa winds (m/s), December–January–February average. Top: LGMa; middle: LGMb–LGMa; bottom: LGMc–LGMb. The shading indicated points for which changes in both components of the wind are significant at the 95% level in a standard Student-T test. The time averages are taken over years 201–250 for LGMa and LGMb, and over years 371–420 for LGMc.

CPD
5, 1055–1107, 2009

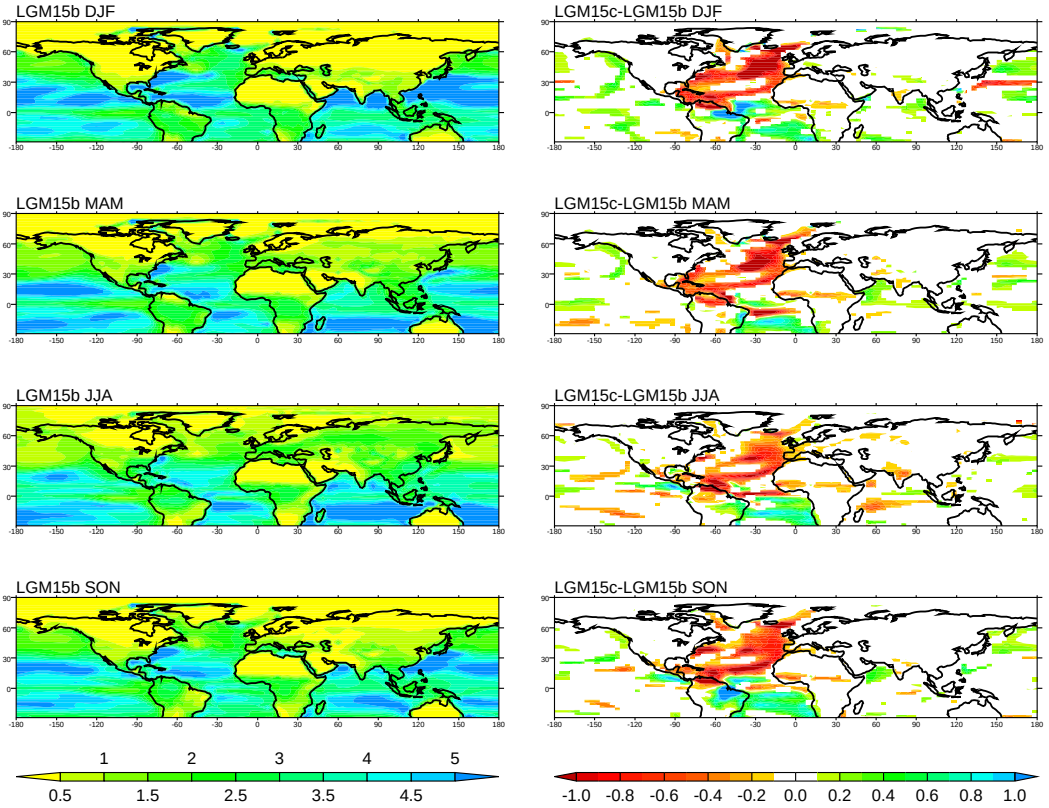

Fig. 14. LGMb evaporation (l.h.s.) and LGMc–LGMb evaporation anomalies (r.h.s) in mm/day for the 4 seasons. The differences have been masked where not significant at the 95% level in a standard Student-T test. The time averages are taken over years 201–250 for LGMb and over years 371–420 for LGMc.

CPD
5, 1055–1107, 2009

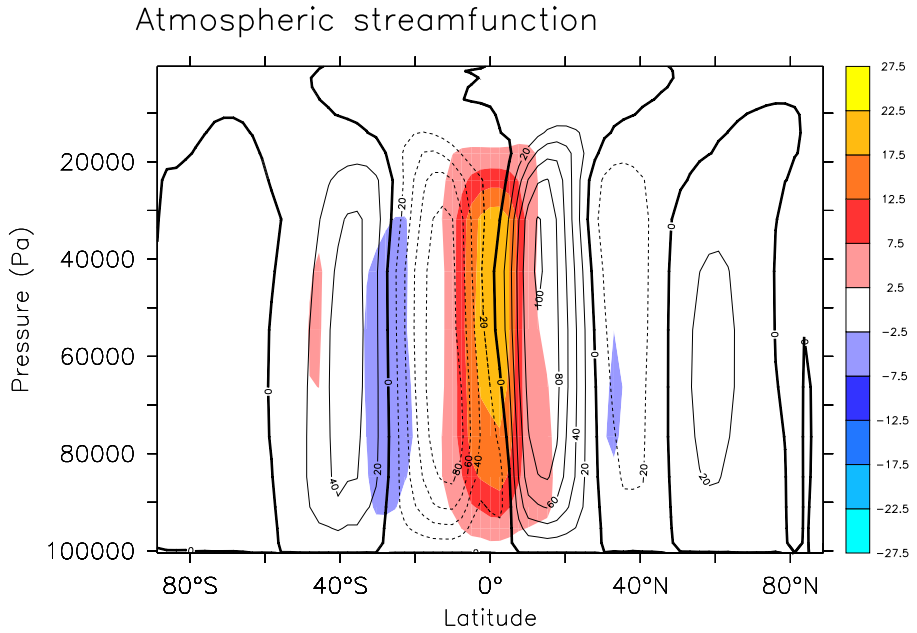

Fig. 15. Meridional atmospheric overturning streamfunction (10^{12} kg/s). The contours represent for the averaged value for LGMb (years 201–250), with a clockwise rotation when positive. Red shaded zones stand for positive (clockwise) differences between LGMc and LGMb (years 371–420 for LGMc, years 201–250 for LGMb). Blue shaded zones stand for negative (anti-clockwise) ones.

CPD
5, 1055–1107, 2009

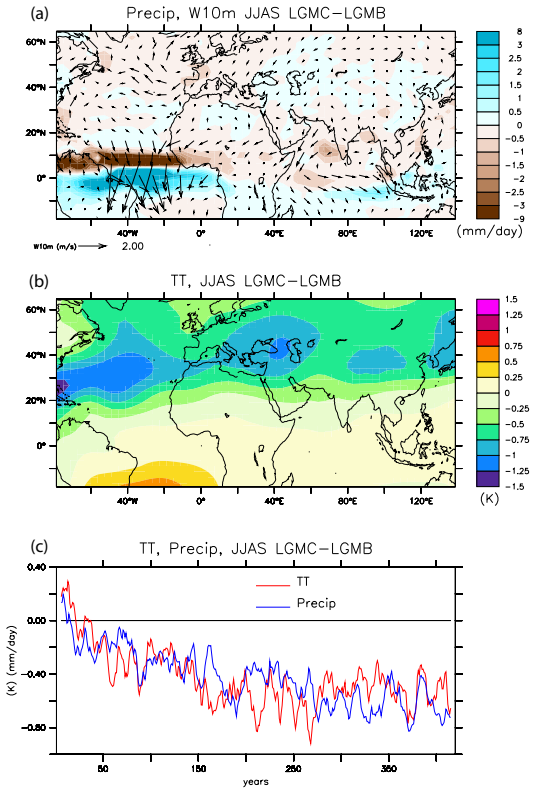

Fig. 16. **(a)** Difference of precipitation (mm/day) averaged for JJAS (June–July–August–September) between the simulations LGMc and LGMb (colours), and of surface winds at 10 m (m/s) (vectors); **(b)** Difference of temperature averaged from 200 to 500 hPa (TT) for JJAS between LGMc and LGMb; for **(a)** and **(b)** the time averages are taken over years 201–250 for LGMb, and over years 371–420 for LGMc, for comparison to other figures; **(c)** Evolution of TT averaged over the region (50°–100° E, 20°–50° N) (red) and of precipitation averaged over the region (60°–80° E, 5°–15° N) (blue) for LGMc minus LGMb (average over years 101–150).

CPD
5, 1055–1107, 2009

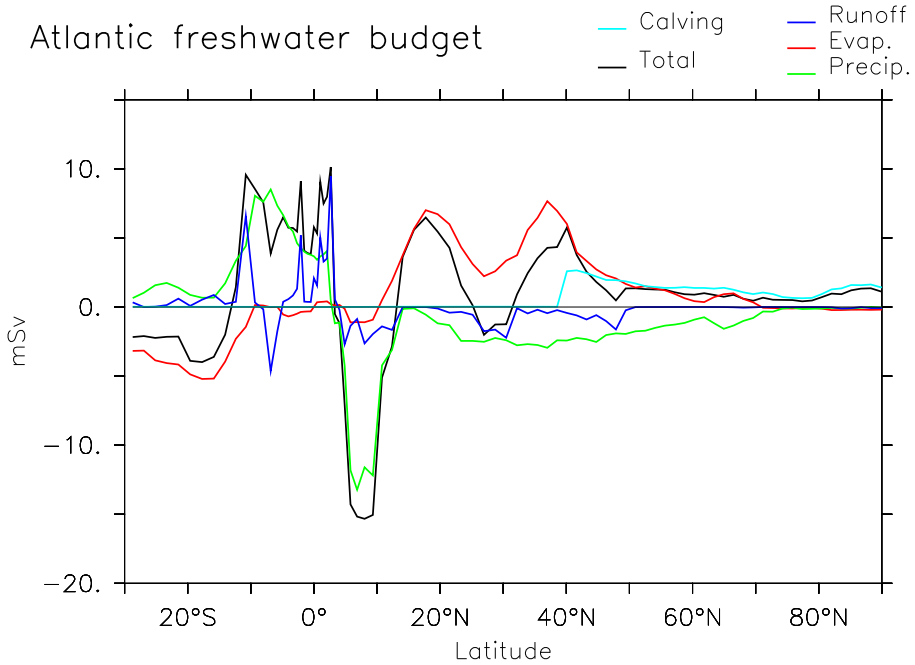

Fig. 17. Freshwater flux differences (LGMc–LGMb), in mSv, zonally summed over the Atlantic. The time averages are taken over years 201–250 for LGMb and over years 371–420 for LGMc. Total flux in black, and calving flux in cyan, runoff in blue, evaporation in red and precipitation in green.